

Generating and receiving OAM electromagnetic waves

Technical work report

submitted to

Lucerne University of Applied Sciences and Arts
Engineering & Architecture
Department of Electrical Engineering

on

June 4, 2016

from

Tobias Plüss, B.Sc.

Lecturers:

Prof. Marcel Joss Advisor

Prof. Dr. Anja Skrivervik Expert

Declaration of academic honesty

The author hereby certifies that this work has been written independently, all the references and resources used have been fully declared and that those parts of the work – including tables, charts and illustrations – which are obtained from other works or from the internet, either literally or analogously, are in any case marked as a borrowing by indication of the source, and that this work has not yet been submitted in the same or a similar form. Unless otherwise noted, illustrations, photos, tables etc. are own works; this document itself is based on a L^AT_EX-template from [9].

Horw, June 4, 2016

the author

Tobias Plüss

Kurzfassung

Elektromagnetische Wellen können verschiedene Arten der Polarisierung aufweisen, u.a. sind dies die zirkuläre oder die elliptische Polarisierung. In aktuellen Kommunikationssystemen werden diese verschiedenen Polarisierungsarten eingesetzt, um eine Mehrfachnutzung der selben Frequenz zu ermöglichen oder um eine bessere Störunterdrückung gegen Fremdsysteme zu erzielen.

Nebst den erwähnten Polarisierungen besitzt eine elektromagnetische Welle aber noch einen weiteren Freiheitsgrad, das sogenannte *Orbital Angular Momentum (OAM)*. Im Vorgängerprojekt wurden die theoretischen Grundlagen von OAM erarbeitet und verschiedene Wege zur Erzeugung entsprechender Wellen aufgezeigt und mit Simulationen verifiziert.

In dieser vorliegenden Arbeit soll das Thema weitergeführt werden. Insbesondere soll untersucht werden, wie mit Hilfe eines Antennenarrays ein gewünschter OAM-Mode erzeugt werden kann. Dies soll mit Simulationen verifiziert und als Laboraufbau realisiert werden. Das Antennenarray soll mit dem Antennen-Messsystem STARLAB ausgemessen werden. Insbesondere soll die Orthogonalität der unterschiedlichen OAM-States $l = \{0, \pm 1, \pm 2, \pm 3\}$ experimentell gezeigt werden.

Abstract

Electromagnetic waves can possess different types of polarisation. These can be, for instance, circular or elliptic polarisation. In current communication systems, these different polarisation possibilities are implemented to allow the use of the same frequency by different subscribers or to improve the suppression of interferences from third-party systems.

Besides the above mentioned polarisations, an electromagnetic wave can have an additional degree of freedom, the so-called *Orbital Angular Momentum (OAM)*. In the previous project, the theoretical aspects of OAM have been illustrated and different ways of how to generate corresponding waves have been shown and were verified by means of simulations.

In this work, the subject is further examined. It shall be investigated how an antenna array could be used to generate a desired OAM mode. This should be verified by means of simulations and it shall be tested in the lab. The antenna array shall be measured and verified by means of the STARLAB antenna measurement system and further, the orthogonality of the different OAM states $l = \{0, \pm 1, \pm 2, \pm 3\}$ shall be shown experimentally.

Contents

Preface	viii
1 Introduction	1
1.1 Goals of this project	2

Part I Theoretical part

2 Phased antenna array basics	5
2.1 Construction	5
2.2 Principle of operation	6
2.3 Model for the OAM state	7
2.3.1 Modelling with spherical waves	8
2.3.2 Polarisation of the OAM states	10
3 Power splitters	13
3.1 Comparison of different topologies	13
3.2 Feed network using splitters	13
3.3 Commercial splitters	16
3.3.1 Evaluation of a MINICIRCUITS splitter	17
4 Orthogonality of OAM states	18

Part II Experiments and results

5 Experiment requirements and description	23
5.1 Operating frequency	23
5.2 Phased array feed network	23
5.3 PCB manufacturing	23
5.4 Experiment goals	24
6 Power splitter design	25
6.1 Procedure to create the PCBs	25
7 Antenna design	29
7.1 Antenna type selection	29
7.1.1 Design and simulation of a patch antenna	29
8 Design and simulation of the antenna array	38
8.1 General construction of the array	38
8.2 Simulation of the antenna array	38

9 Experiment setup and measurements 43

 9.1 Construction of the array 43

 9.2 Measurement of the 3D patterns 44

 9.3 Measurement setup 44

 9.4 Measurement error considerations 46

 9.5 Measurement data 47

 9.6 Interpretation of the measurement results 48

10 Lessons learned and outlook 51

 10.1 Conclusion 52

 10.2 Outlook 52

Part III Appendix

List of Tables 57

List of Figures 59

A Datasheets 60

References 62

Abbreviations and terms 66

Preface

Acknowledgement

My first acknowledgement goes to my advisor Prof. Marcel Joss from the Lucerne University of Applied Sciences and Arts. He is the one who rendered this project possible. I also wish to thank Prof. Dr. Anja Skrivervik from the EPFL Lausanne for being available as co-lecturer. A further acknowledgement goes to Dr. Thomas Graf who supported me with many aspects of the FEM software COMSOL.

Horw, June 4, 2016

the author
Tobias Plüss

Introduction

In the former project, various techniques have been shown to generate an OAM beam. To be more precise, it is a Laguerre-Gauss beam with a specified topological charge l . The topological charge is the number of “twists” in the beam.

These techniques include approaches like

- dielectric lenses,
- holograms,
- and mode convertors.

Besides that, it is also possible to use a circular antenna array to generate beams with a desired topological charge. This has been shown in simulations, e.g. in [25].

The antenna array offers more flexibility in OAM generation. The dielectric lenses, holograms and mode convertors suffer from the fact that they are designed for a fixed topological charge. If one wishes to use multiple different topological charges at the same time, e.g. for diversity or as orthogonal channels, one needs to construct multiple dielectric lenses and use beam splitters to produce the OAM beams, as shown in [38]. It has been proven experimentally that such approaches work, but such a system is inflexible and needs a lot of space since a beam splitter is needed as well as different dielectric lenses.

Compared to that, an antenna array offers some advantages:

- If desired, beam forming can be implemented to improve the directivity of the antenna array.
- The topological charge depends on the phase shift of the feed signals for the array elements [25]. If the phase shift is changed, one can adjust the topological charge of the resulting OAM beam.

Especially the second point is of interest in this work. It is indeed possible to create a network with an electronically adjustable phase shift. If such a network is used in the feed of the array elements, one can electronically change the generated topological charge and thus use it e.g. for modulation.

1.1 Goals of this project

First, the very basics of phased arrays are explained. Then, the the individual components needed to construct such an array shall be described. This includes some type of antenna, as well as a power splitter and a phase shifting network.

After that, an antenna array is simulated using a FEM software. The feed network for the array as well as the array itself is constructed and tested. The measured array pattern is compared with the simulation.

Theoretical part

Phased antenna array basics

This chapter gives a brief introduction to phased antenna array techniques. First, the basic theory of phased array antennas is discussed, and then a short overview of different techniques on how to feed the antennas is given.

2.1 Construction

As the name suggests, an array antenna is constructed from an array of so-called array elements. Fig. 2.1 shows different kinds of how the array elements can be arranged.

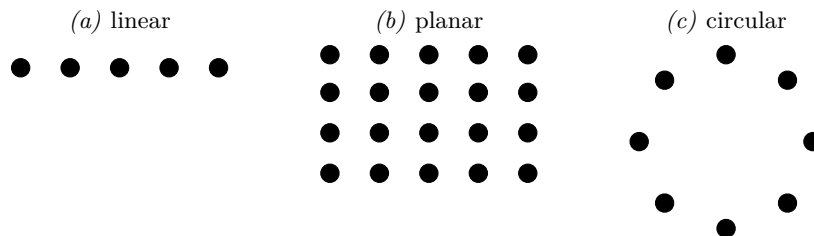


Fig. 2.1. Types of phased arrays

The feed for each array element can be realised in different configurations:

- each element is fed with the same signal (same magnitude and phase). This improves the directivity as well as the gain [10].
- the signals fed to the elements can have a different amplitude (but the same phase). This allows to adjust the main lobe width of the array
- the elements can be fed with a phase-shifted signal (but all with the same magnitude). This is then called a *phased array*.

If the phase shift between the array elements is not fixed but adjustable, it is possible to electronically adjust the direction of the main lobe when transmitting [5, 12] and when receiving it is possible to measure the angle of incidence by measuring the phase shift between the individual antenna signals [20].

2.2 Principle of operation

The principle of operation of a phased array is first explained for the receiver case. Due to the reciprocity property [7, 18] of the antennas, the transmit case is equivalent.

Fig. 2.2 shows a simple linear antenna array with an incident plane wave. Plane waves do not exist in reality, but far away from the transmitting antenna, the spherical waves produced by the antenna can be approximately viewed as plane waves.

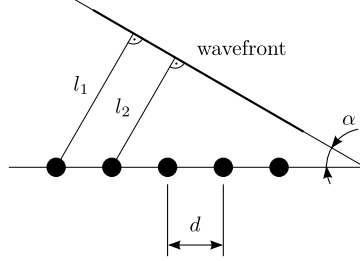


Fig. 2.2. Schematic overview of a linear antenna array

Assume the plane wave is incident to the array at the angle α , as depicted in Fig. 2.2. Then, for the array elements on the left side, the wave front has to travel the additional distance

$$\Delta l = l_1 - l_2 = d \cdot \sin \alpha \quad (2.1)$$

for which the time

$$\Delta t = \frac{\Delta l}{c} \quad (2.2)$$

is needed. This gives a phase shift of

$$\varphi' = \frac{\Delta t}{T} = f \Delta t = \frac{f d \sin \alpha}{c} \quad (2.3)$$

with

$$\frac{f}{c} = \frac{1}{\lambda} \quad (2.4)$$

we thus have:

$$\varphi' = \frac{d \sin \alpha}{\lambda} \quad (2.5)$$

Now assume the array elements are spaced at a distance $d = \lambda$ and the wave is incident at an angle of $\alpha = 90^\circ$. From these conditions, Eqn. 2.5 would yield a phase shift of 1, but actually it should be 2π , so a factor of 2π needs to be included in Eqn. 2.5 from which we get the phase shift relation

$$\varphi = \frac{2\pi d \sin \alpha}{\lambda} \quad (2.6)$$

and with the wavenumber

$$k = \frac{2\pi}{\lambda} \quad (2.7)$$

the phase shift can also be expressed as follows:

$$\varphi = k d \sin \alpha \quad (2.8)$$

In the transmitting case, it is clear now due to the principle of reciprocity that the direction in which the waves propagate away from the antenna can be adjusted by phase shifting the feed signals for the individual array elements according to Eqn. 2.8. If the phase shift between the array element feed signals is φ , the angle will be:

$$\alpha = \arcsin \frac{\varphi}{k d} \quad (2.9)$$

As can be seen from this theory, a linear antenna array allows to adjust the transmitting and receiving angle in one dimension. As a consequence, the angle can be adjusted in two dimensions if a two-dimensional array of antennas is used. Such a configuration allows to transmit (or receive) in any direction in the half space. This is also referenced to as spatial filtering.

Remark

For the analysis of the linear phased array in the transmitting case, the Huygens-Fresnel principle normally used for refraction problems in the optics regime can also be used as a model to explain the angle of the produced wave front [27]. Refer to Fig. 2.3. This figure shows a wave incident to an air-water interface. Each point where the wave fronts of the incident wave strike the interface, a source of a spherical wave can be imagined. These waves propagate into the water domain and the superposition of the many spherical wave fronts produces the resulting plane wave.

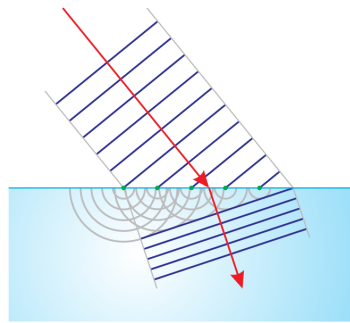


Fig. 2.3. Refraction of a wave at an air-water interface

The arrangement of these small sources of spherical waves at the air-water interface is very similar to a linear phased array.

2.3 Model for the OAM state

Fig. 2.4(a) shows an example of a phased array with 5 elements. Assume that the elements are fed with a signal which is phase-shifted by a constant amount from element to element. This will produce a phase front as indicated in red.

Now imagine that the two array ends – the elements #0 and #4 – are folded together on a circle, as shown in Fig. 2.4(b). The phase front must still have the same phase shift from element to element, but since the elements are arranged on a circular shape, the effect could be compared to the effect of a spiral phase plate with an incident plane wave. The SPP was described in detail in the former project.

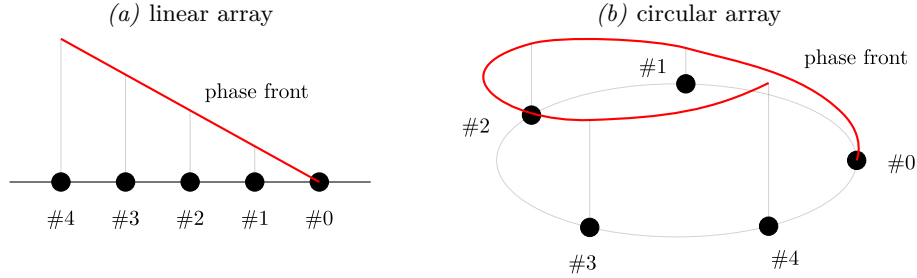


Fig. 2.4. Converting a linear to a circular array

Between the last element (#4 in this case) and the first element (#0), there is a phase front dislocation, as needed for the OAM. This also looks very similar to the SPP. A null is expected in the centre of the circular array because the phase is ambiguous.

If the phase shift of the feed signal is increased, the phase dislocation will also increase and if the sign of the phase shift is inverted, the helicity of the resulting OAM state is also inverted.

Thus, if one manages to electronically control the phase shift, it would be possible to generate different OAM states with the same apparatus.

2.3.1 Modelling with spherical waves

The complex amplitude electric field of a plane wave is given by

$$E = A e^{-j k z} \quad (2.10)$$

if the wave is assumed to travel into positive z direction. Now, z is replaced by

$$z \mapsto \sqrt{x^2 + y^2 + z^2} \quad (2.11)$$

which yields

$$E = A \exp\left(-j k \sqrt{x^2 + y^2 + z^2}\right) \quad (2.12)$$

from Eqn. 2.10. This is the complex amplitude of a spherical wave if A is chosen accordingly: from the Hertz dipole, it can be found [11] that

$$A = \frac{1}{r} = \frac{1}{\sqrt{x^2 + y^2 + z^2}} \quad (2.13)$$

and k is set to 2π in this case for reasons of simplification.

Assume n antennas are arranged as a circular array in the xy -plane at $z = 0$. Each antenna shall produce an electric field with the amplitude given by Eqn. 2.12. If the near-field couplings of these antennas are neglected, the far-fields can simply be added together. For the i -th antenna

$$E_i = \frac{\exp\left(-j 2 \pi \sqrt{(x - x_i)^2 + (y - y_i)^2 + z^2} + j \varphi_i\right)}{\sqrt{(x - x_i)^2 + (y - y_i)^2 + z^2}} \quad (2.14)$$

yields the complex amplitude. Note the additionally introduced phase shift φ_i which is needed to take the feed phase shift into account.

The x - and y -positions of the individual antennas are found with

$$x_i = \varrho \cos \frac{2 \pi i}{n} \quad (2.15)$$

and

$$y_i = \varrho \sin \frac{2 \pi i}{n} \quad (2.16)$$

where ϱ is the circular array radius. With

$$\varphi_i = \frac{2 \pi i}{l} \quad (2.17)$$

the phase shift associated with the OAM state l is found.

The total field produced by all antennas together is then the superposition of the individual fields:

$$E_{\text{tot}} = \sum_{i=0}^{n-1} E_i \quad (2.18)$$

This is then evaluated at a fixed z value ($z = \text{const.}$). Listing 2.1 shows the implementation of this calculation in MATLAB.

The MATLAB code was evaluated for different numbers of elements and for different OAM states. Fig. 2.5 shows a comparison of the resulting figures for different OAM states of an array with four elements. Fig. 2.6 on page 11 shows the different OAM states for an eight element array.

Note that the highest possible OAM state (or topological charge) which can be produced with an array of n elements is

$$-\frac{n}{2} < l_{\text{max}} < \frac{n}{2} \quad (2.19)$$

which is discussed in [4] and explained in detail in [32]. Thus, with a four element array, only the OAM states $l = \{0, \pm 1\}$ can be produced, whereas an eight element array is needed to produce the states $l = \{\pm 3, \pm 2, \pm 1, 0\}$. Theoretically, a 7-element array would suffice to produce the OAM state $|l| = 3$, but 7 elements is an impractical number when the splitter network for feeding the elements is considered, see Sec. 3.2 on page 13.

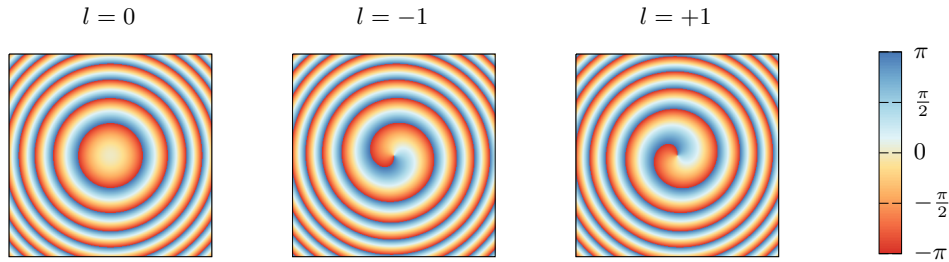


Fig. 2.5. Comparison of different OAM states of a four element array

```

1 elem = 12; % number of elements in the array
2 l = -2; % oam state
3 r = 0.1; % array radius
4 k = 2*pi; % wavenumber
5 ang = (0:1:elem-1)*(2*pi/elem); % angular positions of the elements
6 xpos = r*cos(ang); % element x positions
7 ypos = r*sin(ang); % element y positions
8 phi = l*ang; % phase shift for each element
9 z = 10; % evaluate the total field at this z value
10
11 % anonymous function to calculate the amplitude for one antenna
12 En = @(x, y, z, n) 1./((sqrt((x-xpos(n)).^2+(y-ypos(n)).^2+z.^2).^1) .* ...
13     exp(-1i*k*sqrt((x-xpos(n)).^2 + (y-ypos(n)).^2 + z.^2) + 1i*phi(n));
14
15 [x, y] = meshgrid(linspace(-10, 10, 300), linspace(-10, 10, 300));
16
17 % add all fields together
18 Etot = 0;
19 for n = 1:length(ang)
20     Etot = Etot + En(x, y, z, n);
21 end
22
23 figure(1); pcolor(x, y, angle(Etot)); shading interp; axis square;

```

Listing 2.1. MATLAB script to calculate the OAM states

2.3.2 Polarisation of the OAM states

An OAM state $l \neq 0$ means that the phase of the electric field varies when it is observed on a circular shape around the beam axis. This can be visualised as shown in Fig. 2.7 on page 12. These figures can also be found in [32]. The diagrams show the instantaneous electric field and were produced as follows. Set the electric field to

$$\underline{\mathbf{E}} = \begin{pmatrix} 0 \\ 1 \end{pmatrix} \quad (2.20)$$

and then use the complex amplitude from Eqn. 2.18. The time-dependent electric field can then be written as

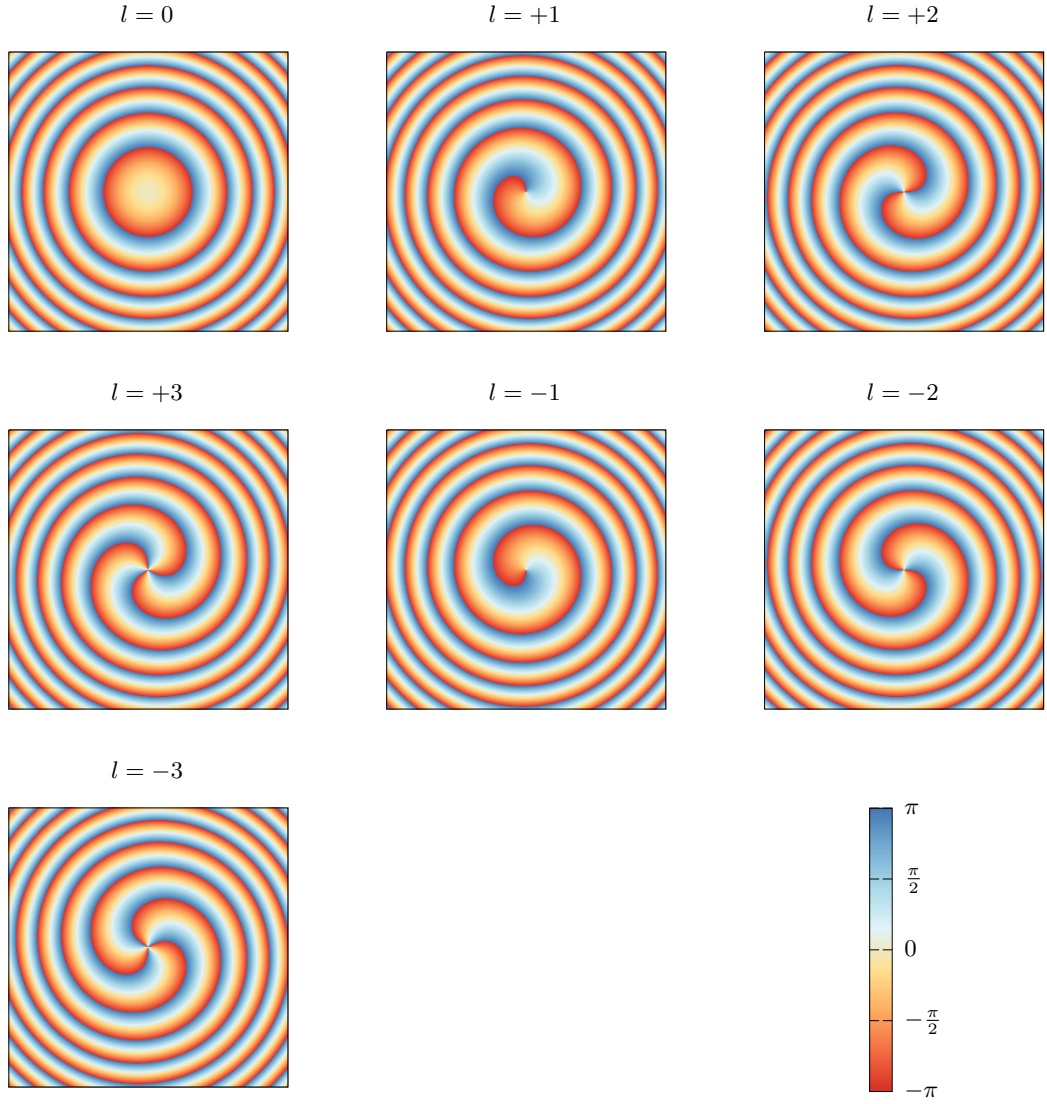


Fig. 2.6. Comparison of different OAM states of a eight element array

$$\mathbf{E} = \sqrt{2} \Re \left(\underline{\mathbf{E}} E_{\text{tot}} e^{j\omega t} \right) \quad (2.21)$$

as shown in [11]. The factor E_{tot} gives rise to the azimuthal phase dependence and $\underline{\mathbf{E}}$ gives the direction of the electric field vectors. When evaluated at $t = 0$, the plots in Fig. 2.7 can be reproduced. The azimuthal phase dependence is even better visible when a circularly polarised electric field is used. Such an electric field can be described with

$$\underline{\mathbf{E}} = \begin{pmatrix} 1 \\ -j \end{pmatrix} \quad (2.22)$$

and it is shown in the last plot in Fig. 2.7. In a “normal” circularly polarised field all the vectors would have the same direction for a given time t , but when the OAM state l is not 0, the phase of the vectors is dependent on the azimuthal angle which gives rise to the different directions of the arrows.

Thus, an OAM carrying wave can have linear polarisation but circular (and thus also elliptic) polarisation is also possible, as [22] shows where a device for generating circularly polarised OAM beams in the optic regime is presented.

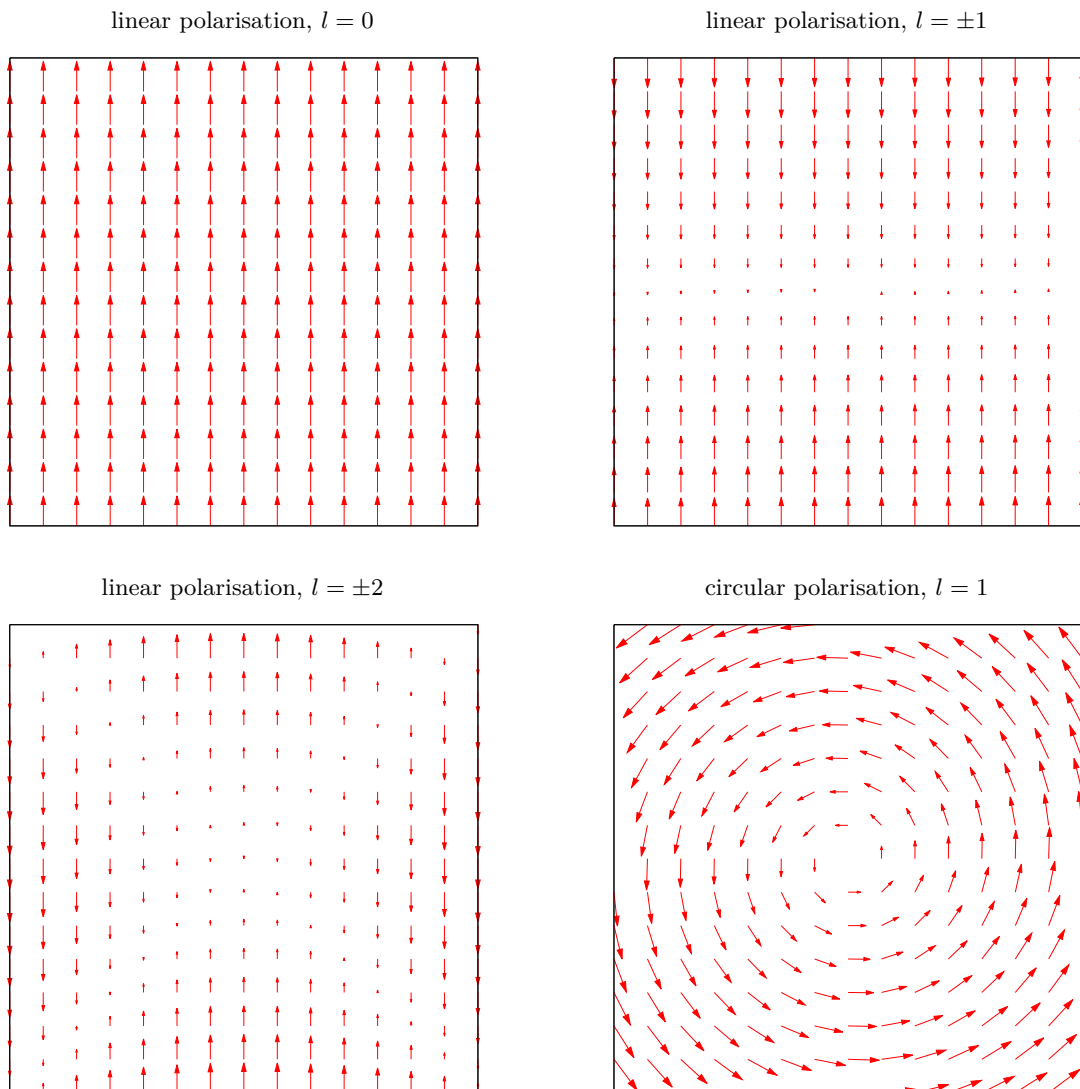


Fig. 2.7. Vector field plots for different OAM states, linear and circular polarisation

Power splitters

A power splitter is a necessary device to build a phased array. This section gives a brief overview of some different power splitter topologies and explains the selection criteria for the power splitter used for the experiment set-up.

3.1 Comparison of different topologies

Tab. 3.1 shows a brief overview of different power splitter topologies [28]. The 2nd column lists the phase shift between the splitter output ports. The 3rd column refers to Fig. 3.1. The Lange coupler is only included in Tab. 3.1 for the sake of completeness. It is not shown in Fig. 3.1 because it is impractical to build due to its need for bond wires to connect the coupling fingers together.

topology	phase	figure
Wilkinson	0°	a
rat race	180° or 0°	b
branch line	90°	c
resistive divider	0°	d
Lange coupler	90°	—

Table 3.1. Overview of splitter topologies and their properties

Note that even though some of the devices in Fig. 3.1 actually have 4 ports. This is because they could be used as directional couplers. If used as a power splitter, the 4th port is an isolated port. It needs to be terminated with a load, though.

3.2 Feed network using splitters

From Tab. 3.1 it is now possible to select a power splitter for the antenna array. As one can see, a branch line coupler as well as a Lange coupler would have a phase

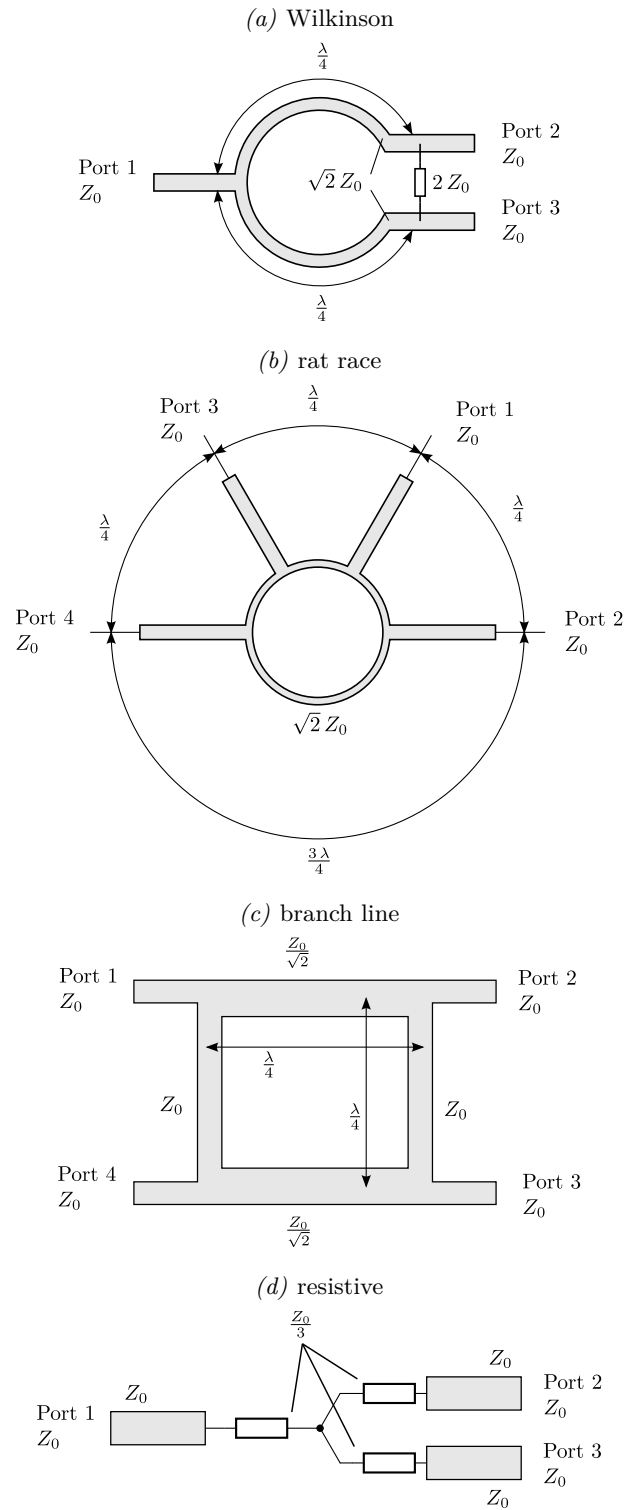


Fig. 3.1. Some topologies of power splitters

difference of 90° between its output signals. This means that additional $\frac{\lambda}{4}$ lines would be needed on the leading- phase port for compensation.

Fig. 3.2 shows the feed network for $N = 8$ antennas. For the sake of simplicity, 0° splitters are assumed. As one can see, the splitters are arranged in a tree structure with

$$L = \frac{\ln N}{\ln 2} = 3 \quad (3.1)$$

levels. The number of splitters at the n -th level is

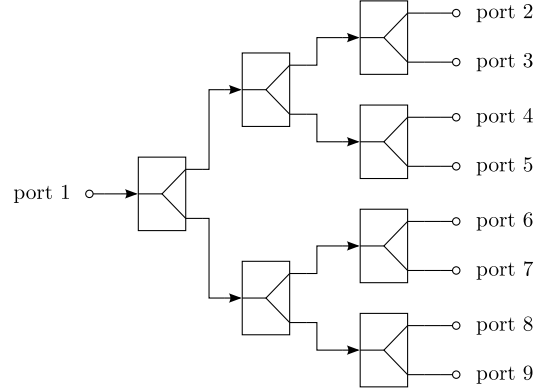
$$N_s = 2^{n-1} \quad (3.2)$$

when the first level has $n = 1$. Thus, for N elements in the array, in total

$$N_{s,\text{tot}} = 2^L - 1 \quad (3.3)$$

splitters are needed. Thus, for an 8-element array, 7 splitters are needed.

Fig. 3.2. An 8-way splitter for the feed network

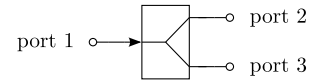


Given the numbering scheme for the ports of an individual splitter as shown in Fig. 3.3, the scattering matrix for a single splitter can be expressed as follows:

$$\mathbf{S} = \frac{k}{\sqrt{2}} \cdot \begin{pmatrix} 0 & 1 & 1 \\ 1 & 0 & 0 \\ 1 & 0 & 0 \end{pmatrix} \quad (3.4)$$

If the splitter is a Wilkinson splitter, then we have $k = j$. If a rat race splitter is used, we have $k = -j$ (if port 4 is properly terminated).

Fig. 3.3. Numbering scheme



In either case, the input signal must flow through L splitters from the input port to one of the output ports. Thus, the output power is

$$\frac{P_{\text{out}}}{P_{\text{in}}} = \left(\frac{k}{\sqrt{2}} \right)^L \quad (3.5)$$

and the total scattering matrix for the feed network may be expressed as follows:

$$\mathbf{S}_{\text{tot}} = \left(\frac{k}{\sqrt{2}} \right)^L \cdot \begin{pmatrix} 0 & 1 & \dots & 1 \\ 1 & 0 & \dots & 0 \\ \vdots & \vdots & \ddots & \vdots \\ 1 & 0 & \dots & 0 \end{pmatrix} \quad (3.6)$$

From this, we find

$$\frac{P_{\text{out}}}{P_{\text{in}}} \approx -9 \text{ dB}$$

for $k = \pm j$ and $L = 3$.

The resistive divider is not of great use for this application. It is easy to construct, but it has major drawbacks. It is a lossy splitter with a loss of 3 dB. Thus, we lose 3 dB in each stage of the splitter, which would result in a total loss of 9 dB for the 8-way splitter. This gives a ratio of

$$\frac{P_{\text{out}}}{P_{\text{in}}} \approx -18 \text{ dB}$$

in this case.

Since the connections between the splitters need to have the same length to achieve the same phase shift, a PCB must have meanders to artificially lengthen the microstrip lines where necessary.

3.3 Commercial splitters

Commercial splitters from the manufacturer MINICIRCUITS are also evaluated. The following selection criteria were used:

- lower operating frequency < 3 GHz
- upper operating frequency > 4 GHz
- the phase difference between the outputs shall be 0° .
- it should be a SMT device to allow mounting on a small PCB. Alternatively it could also have SMA connectors.
- it shall not be a resistive splitter.

Tab. 3.2 shows a summary of devices which were considered suitable for this application.

model no.	type	# of outputs	approx. price [\$]
ZAPD-4-S+	SMA	2	65
ZFSC-2-10G+	SMA	2	70
ZB8PD-4-S+	SMA	8	140
SP-2L+	SMT device	2	1

Table 3.2. Comparison between several commercially available splitters

3.3.1 Evaluation of a MINICIRCUITS splitter

The SP-2L+ device from MINICIRCUITS was considered the most useful device for the splitter network because it offers the smallest footprint and it could easily be integrated on a PCB since it is an SMT device. From its data sheet, which is attached in Appendix A, the transfer characteristics shown in Fig. 3.4 can be extracted. Later, a comparison between this data and a self-made bespoke splitter will be shown.

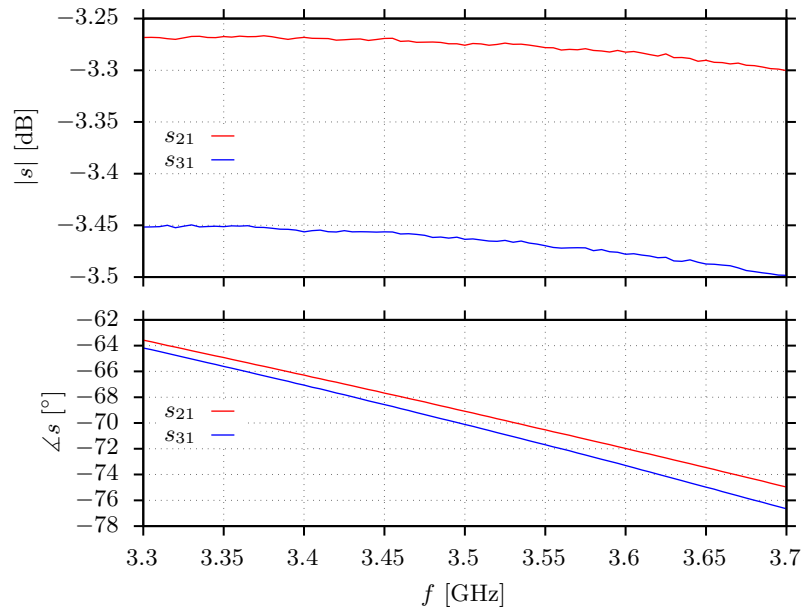


Fig. 3.4. Transmission and reflection characteristics of the MINICIRCUITS device

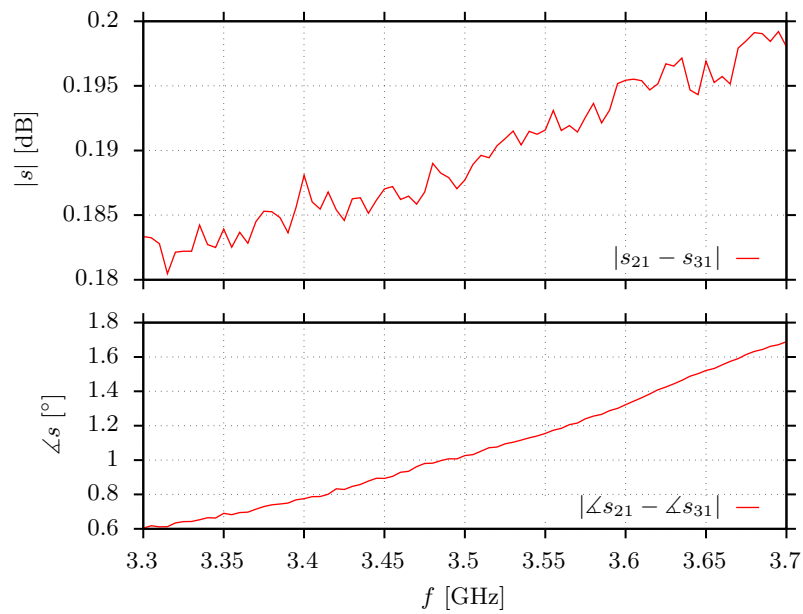


Fig. 3.5. Output balance of the MINICIRCUITS device

Orthogonality of OAM states

The principle of orthogonality means the following: if a transmitter uses an antenna array which works with an OAM state m and a receiver uses an antenna array which is configured for OAM state $n \neq m$, then the receiver will not be able to receive signals from the transmitter. To show this principle, a numerical example is provided.

Assume the transmitter uses OAM state 1 with an 8 element array, e.g. the phase shift of the feed signals for the individual elements is 45° . The receiver uses an exactly identical array. Thus, the signals received by the individual array elements have a phase shift of 45° relative to each other as well. Assuming the received signal has amplitude a , the signal received by the i -th antenna may be described as

$$s_i = a e^{-j\varphi_i} \quad (4.1)$$

where φ_i is the phase shift between the i -th receiving antenna and the feed signal of the transmitting array. From Eqn. 4.1, it is obvious, that if the receiver uses a power combiner with phase shifts of $+\varphi_i$ for each input port, the received total power is given by:

$$s_r = \sum_i a e^{-j\varphi_i} e^{j\varphi_i} = 8 a \quad (4.2)$$

On the other hand, if the receiver uses a power combiner with the “wrong” phase shift, e.g. $-\varphi_i$ as well, then Eqn. 4.1 becomes:

$$s_r = \sum_i a e^{-j\varphi_i} e^{-j\varphi_i} = \sum_i a e^{-2j\varphi} \quad (4.3)$$

From this result, it is not directly obvious that the received signals cancel each other. But refer to Tab. 4.1. It shows the received signal for each antenna and the output signal for a phase network for OAM state +1 and for a phase network for OAM state -1 . As one can see, the first phase network actually compensates the phase shifts of each received signal such that the phase-shifted signals interfere constructively and sum up, this is the case shown Eqn. 4.1. In the other case, if the receiver uses a phase network with the opposite phase shift, one can see that the signals received by antennas #1 and #3 cancel each other, and so do the signals #5 and #7 as well as #2 and #4 and also #6 and #8. Thus, the total output power of a combiner would be zero in this case.

antenna	received signal	phase shift		
		state 1	state -1	state 2
#1	a	$0^\circ \rightarrow a$	$0^\circ \rightarrow a$	$0^\circ \rightarrow a$
#2	$a e^{-j 45^\circ}$	$45^\circ \rightarrow a$	$-45^\circ \rightarrow a e^{-j 90^\circ}$	$90^\circ \rightarrow a e^{j 45^\circ}$
#3	$a e^{-j 90^\circ}$	$90^\circ \rightarrow a$	$-90^\circ \rightarrow -a$	$180^\circ \rightarrow a e^{j 90^\circ}$
#4	$a e^{-j 135^\circ}$	$135^\circ \rightarrow a$	$-135^\circ \rightarrow a e^{j 90^\circ}$	$-90^\circ \rightarrow a e^{j 135^\circ}$
#5	$-a$	$180^\circ \rightarrow a$	$-180^\circ \rightarrow a$	$0^\circ \rightarrow -a$
#6	$a e^{j 135^\circ}$	$-135^\circ \rightarrow a$	$135^\circ \rightarrow a e^{-j 90^\circ}$	$90^\circ \rightarrow a e^{-j 135^\circ}$
#7	$a e^{j 90^\circ}$	$-90^\circ \rightarrow a$	$90^\circ \rightarrow -a$	$180^\circ \rightarrow a e^{-j 90^\circ}$
#8	$a e^{j 45^\circ}$	$-45^\circ \rightarrow a$	$45^\circ \rightarrow a e^{j 90^\circ}$	$-90^\circ \rightarrow a e^{-j 45^\circ}$

Table 4.1. Numerical results

As another example, consider that a phase network with 90° phase shift is used at the receiver, e.g. this would be for OAM state 2. This situation is also shown in Tab. 4.1. It is easily shown that the signals #1 and #5, #2 and #6, #3 and #7 and #4 and #8 cancel each other, so the received power after the combiner will be zero as well. Thus, receiving an OAM state which is produced with a 45° phase shift between the elements at the transmitter side is only possible if the received uses the exact same phase shift. This example shows that different OAM states are indeed orthogonal to each other.

Experiments and results

Experiment requirements and description

5.1 Operating frequency

The operating frequency for any experiments has been chosen at 3.5 GHz. It lies deliberately outside any ISM bands to avoid interferences with WLAN and other ISM services since a shielded measuring chamber is not available.

5.2 Phased array feed network

The power splitter(s) should have no phase shift between the output ports. This is to allow simpler cabling. If the power splitters do have a phase shift between the two output ports, special care must be taken when connecting the array elements to the splitters. In order to compensate for the phase shifts, cables of different lengths must be used. To avoid such complicated cabling, a 0° power splitter is needed.

Further, the power shall be evenly distributed between the output ports such that each array element is fed with the same output power.

5.3 PCB manufacturing

Three different materials are available for manufacturing PCBs:

- standard FR4 material
- Rogers RO3210 low-loss high-frequency material with high ϵ_r
- Rogers RO4350B low-loss high-frequency material with low ϵ_r

Tab. 5.1 shows the parameters of the various base materials. The loss tangent is modelled in COMSOL using a complex permittivity. In [11], the definition

$$\tan \delta = \frac{\epsilon_r''}{\epsilon_r'} \quad (5.1)$$

is found. Thus, with

$$\epsilon_r = \epsilon_r' - j \epsilon_r'' = \epsilon_r' (1 - j \tan \delta) \quad (5.2)$$

the complex permittivity can be found.

PCBs made from FR4 are manufactured as multilayer PCBs with 4 layers. This allows for a very thin dielectric thickness between the top layer and the inner ground layer.

parameters	symbols	values for			units
		RO4350B	RO3210	FR4	
permittivity	ϵ_r'	3.66	10.8	4.35	—
copper thickness		17.5	17.5	35	μm
dielectric thickness	h	1.524	0.64	0.3	mm
loss tangent	$\tan \delta$	0.0037	0.0027	—	—

Table 5.1. Specification of the available base materials for PCBs

5.4 Experiment goals

The experiment's goal is to measure the 3D antenna pattern of circular arrays with OAM state $l = \{0, 1, 2, 3\}$. This is to verify the presence of the deep null in the centre of the pattern in the case of $l \neq 0$ and the absence of the null in case of $l = 0$. Due to reasons of symmetry, it is sufficient if all the positive or all the negative OAM states are measured.

Further, after the pattern is compared with the simulation, two identical arrays are placed in front of each other. By means of a network analyser, the transfer function between the transmitting array and the individual elements of the receiving array is to be measured to prove for the orthogonality of the OAM states.

Power splitter design

A PCB has been designed around the MINICIRCUITS splitter device. The PCB is designed using ALTIUM DESIGNER and is manufactured in 4 different variants: one each with 0° , 45° , 90° and 135° phase shift between two adjacent output ports. This allows to produce the OAM states $l = \{0, \pm 1, \pm 2, \pm 3\}$.

6.1 Procedure to create the PCBs

The 0° splitter is easily constructed. The 0° phase shift is achieved by equal trace lengths for each splitter output, assuming that all MINICIRCUITS splitter devices have an almost identical phase shift. In Fig. 6.1 one can see the absolutely symmetric layout where all the traces are of equal length. Refer to Fig. 6.3 on page 28 for some photographs.

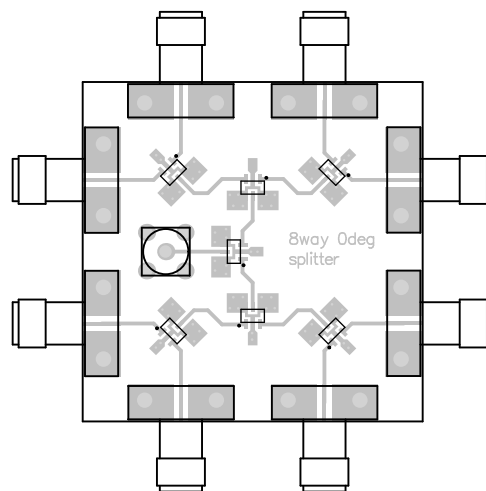


Fig. 6.1. CAD drawing of the 0° splitter

The splitters with a phase shift $\neq 0$ between the output ports are designed using meandered microstrip lines. The design procedure was an iterative process as follows:

- Calculate the correct trace length using AWR MICROWAVE OFFICE. This yields the $\frac{\lambda}{4}$ trace length, which equals 90° . The result was 11.88 mm.

- Manufacture a splitter PCB whose trace lengths are increasing in steps of 11.88 mm.
- Measure the phase difference between the output ports. The measured mean phase shift was 83° . Thus, the 90° trace length was increased by a factor of

$$\frac{90^\circ}{83^\circ} \approx 1.08$$

which yields a new length difference of ≈ 12.7 mm for 90° phase shift. The trace length difference for 45° phase shift thus is 6.34 mm and the one for 135° is 19.02 mm.

- A new PCB is manufactured with the corrected trace lengths.

Fig. 6.2 shows the CAD drawings of the 4 PCB variants. One can clearly identify the meandered lines. Tab. 6.1 shows the measured forward transmission characteristics of the different splitter variants.

	0° variant		45° variant		90° variant		135° variant	
	$ s_{ij} $ [dB]	$\angle s_{ij}$ [°]	$ s_{ij} $ [dB]	$\angle s_{ij}$ [°]	$ s_{ij} $ [dB]	$\angle s_{ij}$ [°]	$ s_{ij} $ [dB]	$\angle s_{ij}$ [°]
s_{10}	-11.2	90.8	-11.2	92.8	-11.5	90.9	-13.2	-102
s_{20}	-11.2	91.4	-11.3	51.1	-11.6	3.1	-14	122
s_{30}	-11.1	91.3	-11.3	9.1	-12.0	-88.2	-14	-6
s_{40}	-11.0	91.9	-11.4	-35.0	-12.1	-178.2	-14	-147
s_{50}	-10.9	92.5	-11.6	-82.2	-12.3	99.2	-13	72
s_{60}	-10.9	91.3	-11.8	-129.2	-12.5	9.2	-15	-61
s_{70}	-11.2	88.5	-12.0	-170.9	-12.8	-78.8	-15	169
s_{80}	-11.2	88.9	-12.0	146.8	-13.1	-177.5	-15	25

Table 6.1. Magnitude and phase of the manufactured splitters

In Tab. 6.2, the phase differences between the output ports calculated from the measurements shown in Tab. 6.1 are shown.

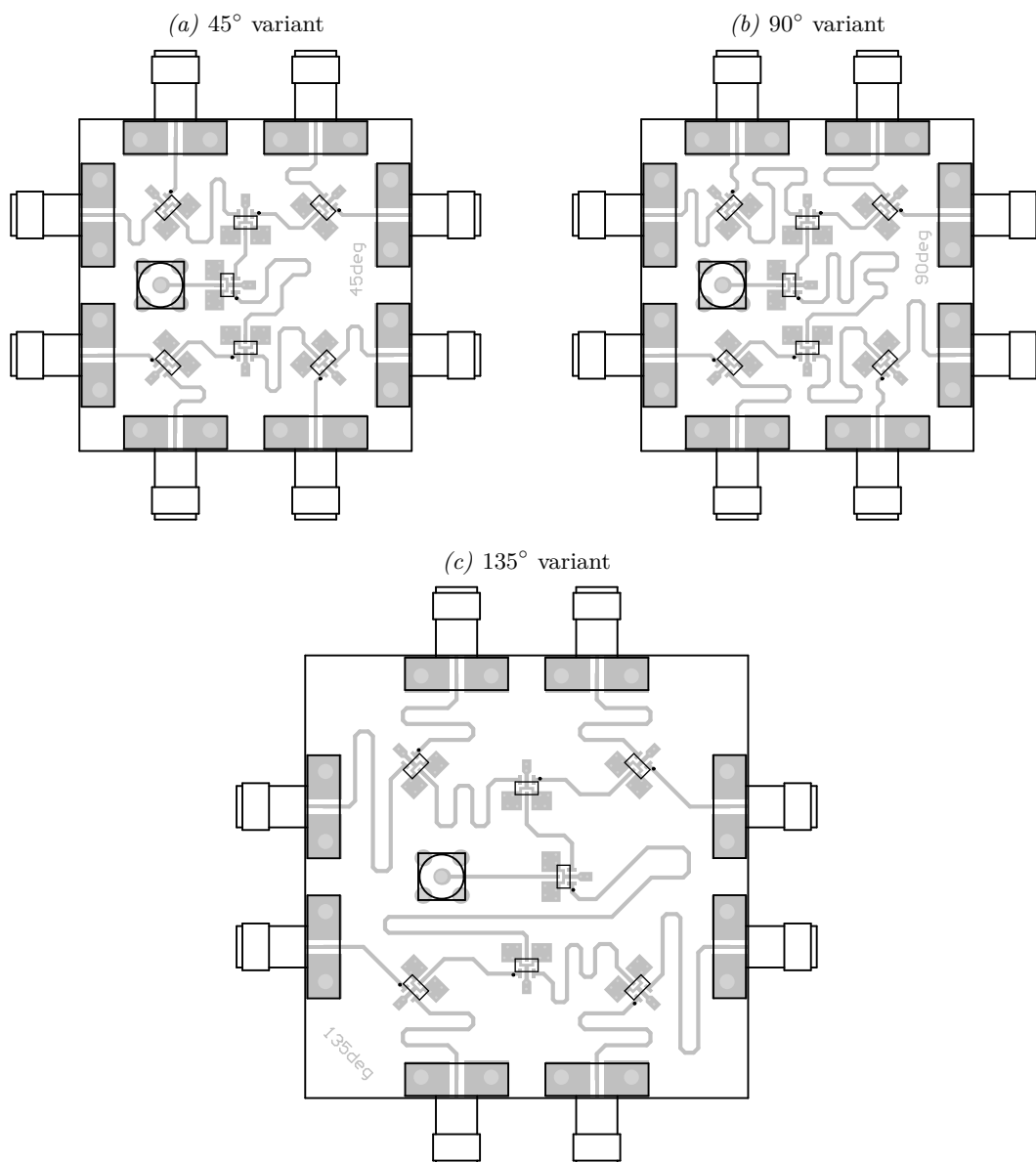
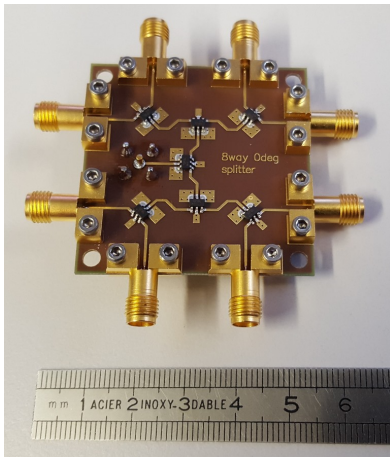
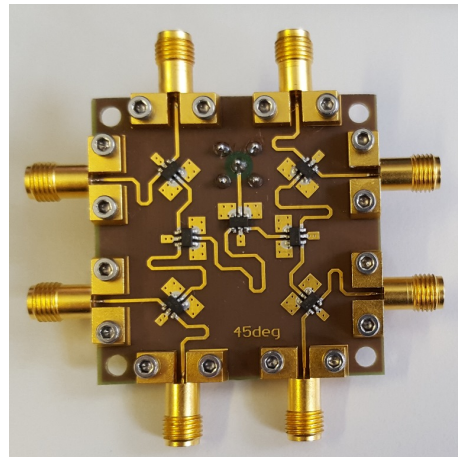
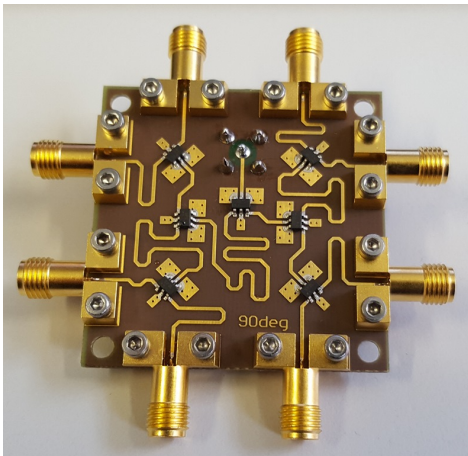
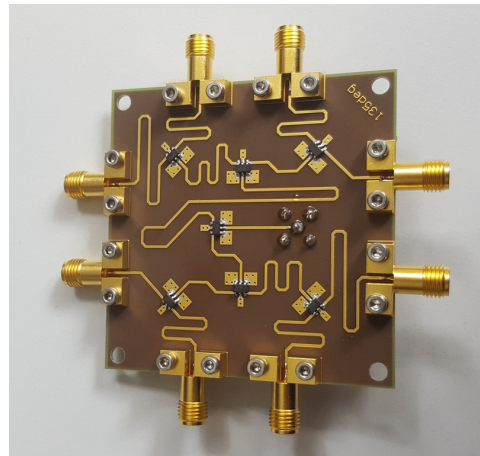


Fig. 6.2. CAD drawings of the different PCB variants, to scale

ports	splitter variant			
	0°	45°	90°	135°
$ \angle s_{10} - \angle s_{20} $	0.6°	41.7°	87.8°	136°
$ \angle s_{20} - \angle s_{30} $	0.1°	42°	91.3°	128°
$ \angle s_{30} - \angle s_{40} $	0.6°	44.1°	90°	141°
$ \angle s_{40} - \angle s_{50} $	0.6°	47.2°	82.6°	141°
$ \angle s_{50} - \angle s_{60} $	1.2°	47°	90°	133°
$ \angle s_{60} - \angle s_{70} $	2.8°	41.7°	87.8°	130°
$ \angle s_{70} - \angle s_{80} $	0.4°	42.3°	98.7°	144°
$ \angle s_{80} - \angle s_{10} $	0.8°	54°	91.6°	127°
mean	0.887°	45°	89.9°	135°

Table 6.2. calculated phase difference between the output ports of the splitters

(a) 0° splitter(b) 45° splitter(c) 90° splitter(d) 135° splitter**Fig. 6.3.** Photographs of the manufactured splitters

Antenna design

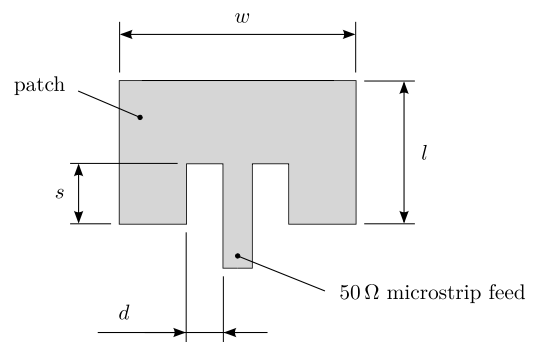
7.1 Antenna type selection

There are different possibilities for the antenna type, for instance dipoles, monopoles or patches, to name a few. For the first experiments, the antenna and the corresponding feed network should be as simple as possible. For this reason a patch antenna is constructed for the first experiment. It allows easy matching to $50\ \Omega$ and it does not need a balun for the feed. Instead it can be directly fed with a $50\ \Omega$ microstrip line.

7.1.1 Design and simulation of a patch antenna

Fig. 7.1 shows the geometry of the patch antenna. It is a variant with an inset feed, meaning that the feed line is inset into the patch by a certain distance s , allowing for a better matching to $50\ \Omega$.

Fig. 7.1. Geometry of the patch antenna with inset microstrip feed



This type of patch antenna produces a field which is linearly polarised along the dimension l . To show this, refer to Fig. 7.2. In subfigure (a) a schematic 3D view of a patch antenna on a substrate is shown as well as the orientation of the x , y and z axes. Then, in subfigure (b), a xz cut through this arrangement is shown.

Since the two ends of the patch antenna are open-circuited, the electric field must have its maximum value on these two ends. This is represented by the arrows. Due to the fringing field whose field lines start on the top of the antenna, the polarisation of the radiated field must be parallel to the x axis. The 3D view of the electric field

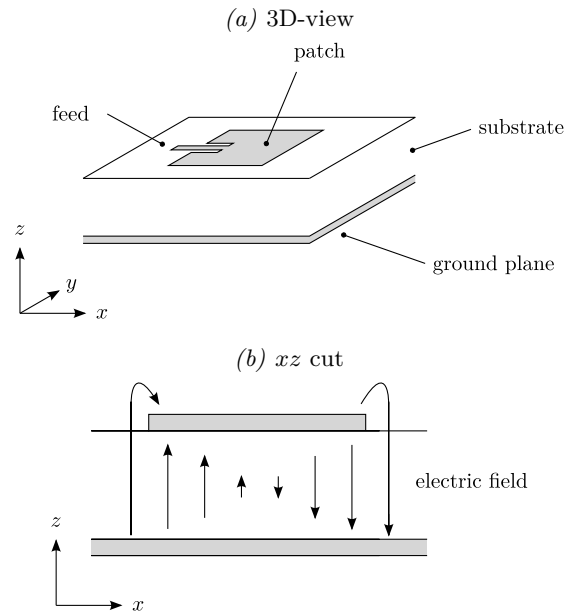


Fig. 7.2. Analysis of the polarisation of a patch antenna

computed with a COMSOL simulation is shown in Fig. 7.3 and indeed, as one can see, the polarisation is along the x axis.

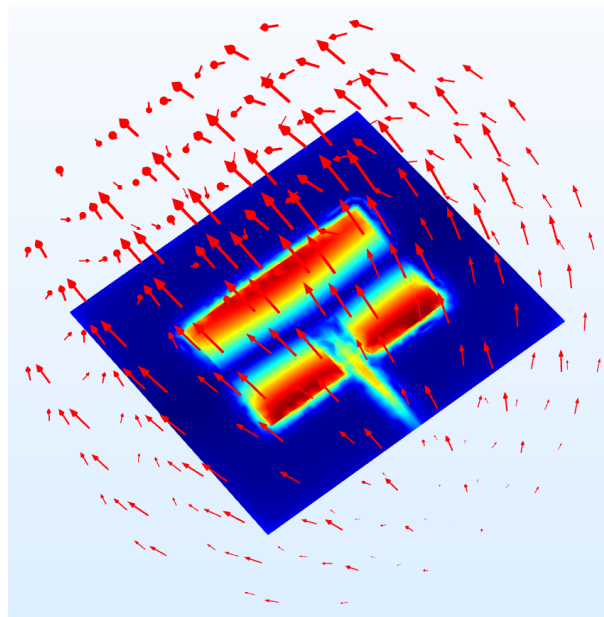


Fig. 7.3. Polarisation of the patch antenna

The design equations for the microstrip patch antenna can be found in [10, 13]. For the sake of simplicity, the design procedure is explained here as well. The width w of the patch is given by:

$$w = \frac{c}{2f} \cdot \sqrt{\frac{2}{\epsilon_r + 1}} \quad (7.1)$$

Second, the effective ϵ_r is calculated. This number is dependent on the geometry of the conductor. Because some electric field lines go through the air and some go

through the substrate, the effective ϵ_r is somewhat lower than the ϵ_r of the substrate. For the microstrip patch it can be found using following equation:

$$\epsilon_{r,\text{eff}} = \frac{\epsilon_r + 1}{2} + \frac{\epsilon_r - 1}{2} \cdot \frac{1}{\sqrt{\left(1 + \frac{12h}{w}\right)}} \quad (7.2)$$

In the next step, the dimension Δl has to be calculated. At the edges of the patch, there is some fringing electric field and Δl is an approximation on how much larger this electric field is than the patch:

$$\Delta l \approx 0.412 h \frac{(\epsilon_{r,\text{eff}} + 0.3) \left(\frac{w}{h} + 0.264\right)}{(\epsilon_{r,\text{eff}} - 0.258) \left(\frac{w}{h} + 0.8\right)} \quad (7.3)$$

Further, from the desired frequency of operation, the effective length of the path is found by:

$$l_{\text{eff}} = \frac{c}{2 f \sqrt{\epsilon_{r,\text{eff}}}} \quad (7.4)$$

Note that the effective length is slightly longer than the “real” length of the copper structure because of fringing electric fields at the edges of the copper patch. Thus, to find the real length of the patch, the length of the fringing field needs to be subtracted:

$$l \approx l_{\text{eff}} - 2 \Delta l \quad (7.5)$$

These equations then give the rough dimensions of the patch. The inset feed is found by means of optimisation. An initial guess for the inset feed can be found with

$$s \approx l \cdot \frac{c_7 \epsilon_r^7 + c_6 \epsilon_r^6 + c_5 \epsilon_r^5 + c_4 \epsilon_r^4 + c_3 \epsilon_r^3 + c_2 \epsilon_r^2 + c_1 \epsilon_r + c_0}{2 \cdot 10^4} \quad (7.6)$$

with the parameters c_i chosen according to Tab. 7.1.

parameter	value
c_7	0.001699
c_6	0.13761
c_5	-6.1783
c_4	93.187
c_3	-682.69
c_2	2561.9
c_1	-4043
c_0	6697

Table 7.1. Polynomial coefficients for the inset feed calculation

The distance d should be as small as possible, but large enough to minimise the coupling of the strong electric field at the patch edge to the feed line. A starting point can be found with

$$d > w_s \quad (7.7)$$

```

1 % specify parameters of the substrate and the desired frequency
2 f = 3.5e9; % frequency [Hz]
3 h = 0.64e-3; % dielectric thickness [m]
4 er = 10.8; % dielectric constant
5 c = 3e8; % speed of light [m/s]
6
7 % calculate the dimensions
8 w = c/(2*f)*sqrt(2/(er+1));
9 ereff = (er+1)/2 + (er-1)/2/sqrt(1+12*h/w);
10 dl = 0.412*h*(ereff+0.3)*(w/h+0.264)/((ereff-0.258)*(w/h+0.8));
11 leff = c/(2*f*sqrt(ereff));
12 l = leff-2*dl;
13
14 % polynomial coefficients for the inset feed
15 c = [0.001699 0.13761 -6.1783 93.187 -682.69 2561.9 -4043 6697];
16
17 % inset feed
18 s = polyval(c, er) * 1/2 * 1e-4;
19
20 % print the values
21 fprintf('w=%0.1f mm, l=%0.1f mm\n', w*1000, l*1000);
22 fprintf('inset feed: %0.1f mm\n', s*1000);

```

Listing 7.1. MATLAB script to calculate the patch antenna dimensions

where w_s is the width of the feed line.

A MATLAB program has been implemented to automatically calculate these values since the process is somewhat elaborate. Listing 7.1 shows the MATLAB code. The parameters of the substrate and the desired operating frequency can be specified on lines 2 to 4. The code then prints the calculated parameters in the following format:

```

w=17.6 mm, l=13.0 mm
inset feed: 6.1 mm

```

To verify the parameters calculated with the MATLAB script, a full-wave simulation is done using COMSOL as well as EMPIRE. This also allows for optimisation of the parameters. Following simulations were done:

- a parametric sweep of the parameters s , w , d and l to find the values which minimise the $|s_{11}|$ scattering parameter, i.e. which give the best match to 50Ω .
- a frequency sweep to analyse $|s_{11}|$ as a function of the frequency.
- a far-field calculation at 3.5 GHz to find the antenna pattern.

Different variants of the patch antenna are calculated using the MATLAB program. Tab. 7.2 shows the parameters of the variants. The microstrip parameters are found using the procedures described in [15] and [33].

parameters	symbols	values for			units
		RO4350B	RO3210	FR4	
width	w	28.1	17.6	25.8	mm
length	l	21.9	13.0	20.2	mm
feed clearance	d	4	1.2	1.1	mm
feed inset	s	6.3	6.1	6.2	mm
50 Ω microstrip width	w_s	3.3	0.55	0.53	mm

Table 7.2. Calculated dimensions for the patch antenna variants

Using these values as a starting point, the return loss $|s_{11}|$ was simulated using a full-wave simulation in EMPIRE and the antenna pattern was simulated using COMSOL. The losses of the dielectric and the conductors are neglected in this simulation. Refer to Fig. 7.4 for the results.

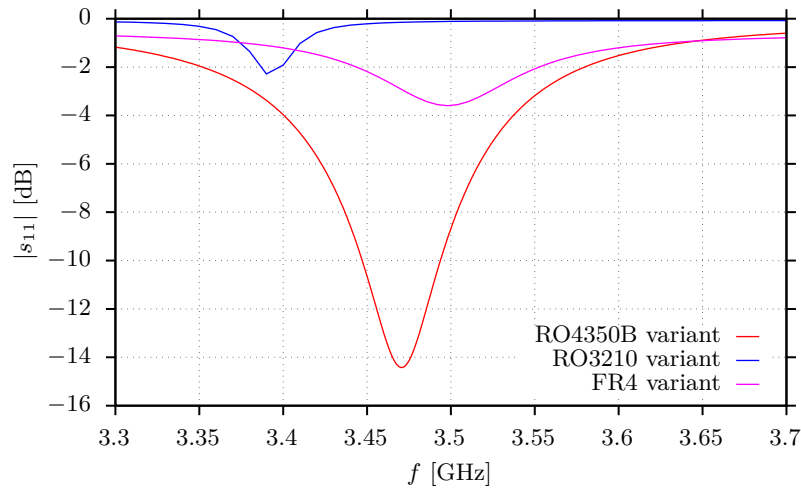


Fig. 7.4. Simulated return loss of the patch antenna variants

As one can see, the MATLAB script gives only a ballpark figure for the antenna dimensions. The optimal parameters for w , l , d and s have been found by means of parametric sweeps and minimisation of $|s_{11}|$. This leads to the optimised geometry with the parameters shown in Tab. 7.3.

parameters	symbols	values for			units
		RO4350B	RO3210	FR4	
width	w	27.3	15.9	26.1	mm
length	l	21.8	12.75	20.2	mm
feed clearance	d	3.8	1.1	1.6	mm
feed inset	s	6	5.1	3.5	mm

Table 7.3. Optimised dimensions

The simulated return loss graphs for the optimised geometries are shown in Fig. 7.5. For comparison, the original curves are plotted as well (dashed).

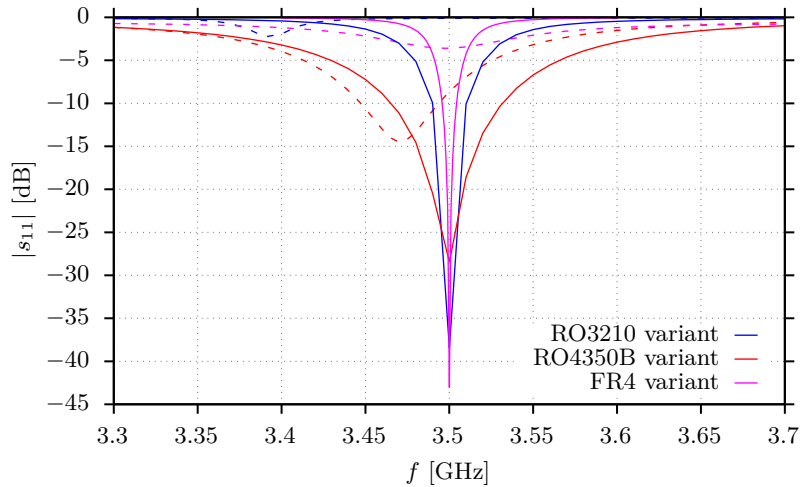


Fig. 7.5. Comparison of the return loss of the original (dashed lines) and the optimised patch antenna geometries (straight lines)

After the simulation, the antenna has been manufactured. It has been decided to produce the antennas on FR4 substrate. This has the advantage that the repeatability as well as the quality of the conductor surface is much better, even though FR4 has the disadvantage of a higher loss tangent and the dielectric constant is now known so well. Fig. 7.6 shows a photograph of the printed circuit boards. They were manufactured at PCB-Pool which allows to use precisely etched structures.

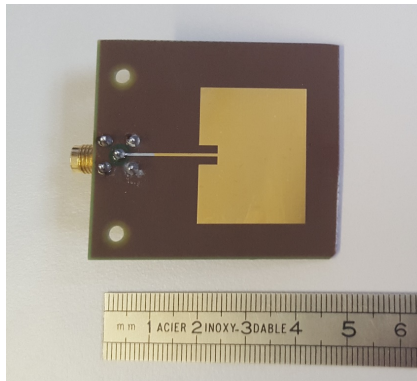


Fig. 7.6. Photograph of the manufactured patch antenna

The scattering parameters of the manufactured patch antenna are then measured using a HP 8753C network analyser which can be controlled from MATLAB using GPIB. Fig. 7.7 shows the s_{11} measurement result.

A significant frequency offset can be observed. The resonant frequency is at 3.73 GHz instead of the desired 3.5 GHz. Further, the measured dip at the resonant frequency is not as deep as predicted by the simulation. The reason for this is that the dielectric constant as well as the loss tangent of the FR4 material used are not known precisely

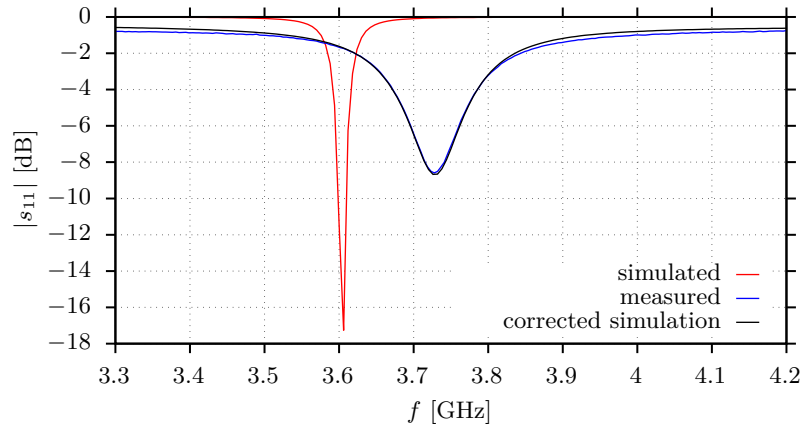


Fig. 7.7. Measured scattering parameter of the manufactured antenna

enough for this frequency. To model these parameters more accurately, they are adjusted in the simulation whilst the geometry was kept fixed until the simulation shows approximately the same results as the measurement. Thus, the simulation is corrected such that it better reflects the reality. This is shown in Fig. 7.7 with the black line.

At this point, the dielectric constant and the loss tangent of the FR4 material are considered as known. The simulation gives the values $\epsilon_r = 3.845$, $\tan \delta = 0.027$. With these new values, a further optimisation of the patch antenna is performed. Tab. 7.4 shows the new dimensions.

parameters	values	units
w	16.4	mm
l	21.85	mm
d	1.6	mm
s	2.25	mm

Table 7.4. Dimensions of the redesigned patch antenna

Fig. 7.8 shows a photograph of the redesigned patch antenna. Refer to Fig. 7.6 for comparison.

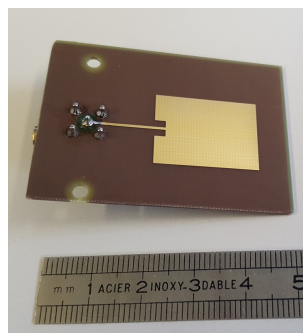


Fig. 7.8. Photograph of the redesigned patch antenna

In Fig. 7.9, the $|s_{11}|$ measurement is shown for the optimised patch antenna. It is not as optimal as the simulation promises, but this could be due to manufacturing tolerances. The patch antenna is extremely sensitive to variations of the length l , as has been found in the simulations.

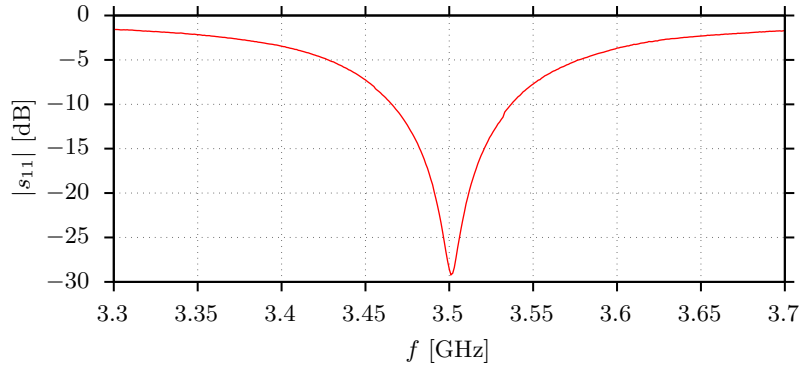


Fig. 7.9. Measured scattering parameter of the manufactured antenna

In the next step, the radiation pattern of the patch antenna is measured. For this purpose, the STARLAB antenna measurement system is used. Fig. 7.10 shows how the radiation pattern is measured.

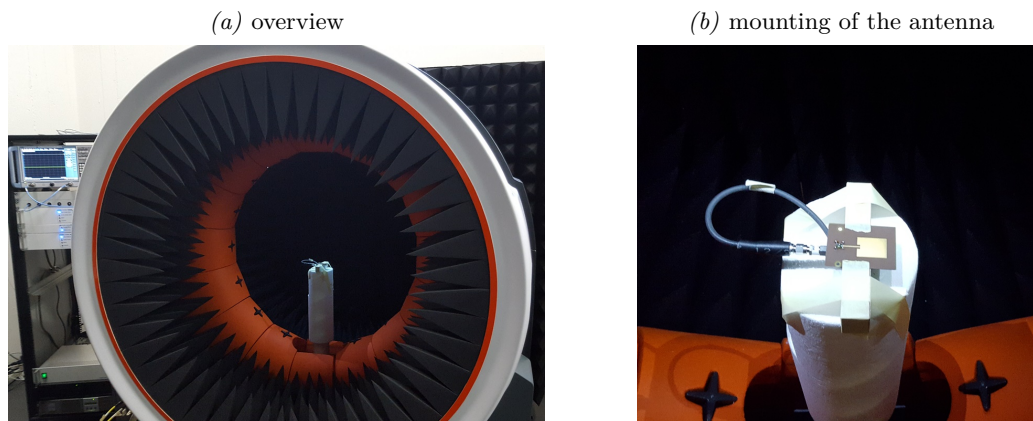


Fig. 7.10. How the antenna radiation pattern is measured

The measurement result is shown in the graph in Fig. 7.11. It is normalised to 0 dB. The pattern is in good accordance with the theory described in [36].

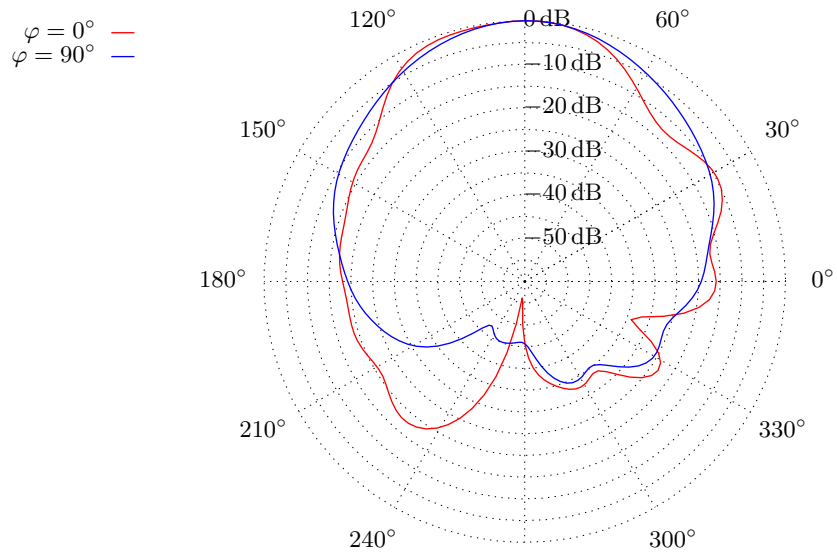


Fig. 7.11. Measured radiation pattern of the patch antenna

Design and simulation of the antenna array

8.1 General construction of the array

According to [25] a circular array of antennas is used. If there are n antennas,

$$\alpha = \frac{2\pi}{n} \quad (8.1)$$

is their angular displacement. In order to produce a desired OAM state with topological charge $\pm l$, the feed signals for the individual antennas need to be shifted in phase by the angle

$$\Delta\varphi = \pm \frac{2\pi l}{n} \quad (8.2)$$

which can also be found in [25]. Further, the array should have a diameter less than or equal to λ . For this application it means that the array diameter should be in the order of magnitude of

$$D = \lambda \approx 85.7 \text{ mm}$$

which gives a limitation on the number of array elements if their size is given. In [25], circular arrays with diameter λ are used, whereas [4] uses an array of diameter 0.6λ .

In general, if a large number of array elements is needed, the antennas need to be small or the array diameter needs to be increased, otherwise the antennas would touch each other.

According to [25], the number of elements should be $n \geq 6$. Otherwise, a ripple is observed in the radiation pattern. This is the reason why 8 elements will be used for the experiment.

8.2 Simulation of the antenna array

The array consists of eight elements arranged in a circle of radius 45 mm. Fig. 8.1 shows how the array is oriented with the x , y and z axes. The same axis orientation is used for the array pattern plots as well.

The OAM mode is varied between -2 and 2 . Fig. 8.2 shows qualitative patterns of the electric far field norm for the OAM states 0 in plot (a), for $+1$ in plot (b) and for

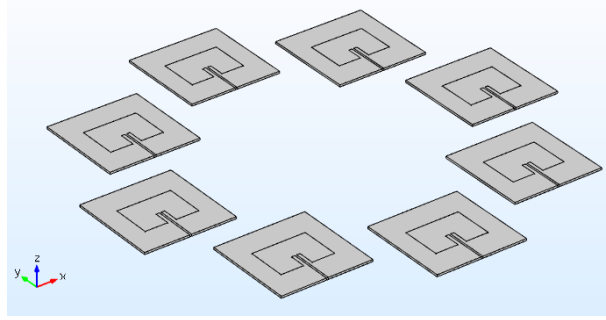


Fig. 8.1. Orientation of the array for the simulation

+2 in plot (c). The patterns for the -1 and -2 states look the same. As expected, the state 0 does not have a null in its centre, whereas states 1 and 2 do have one.

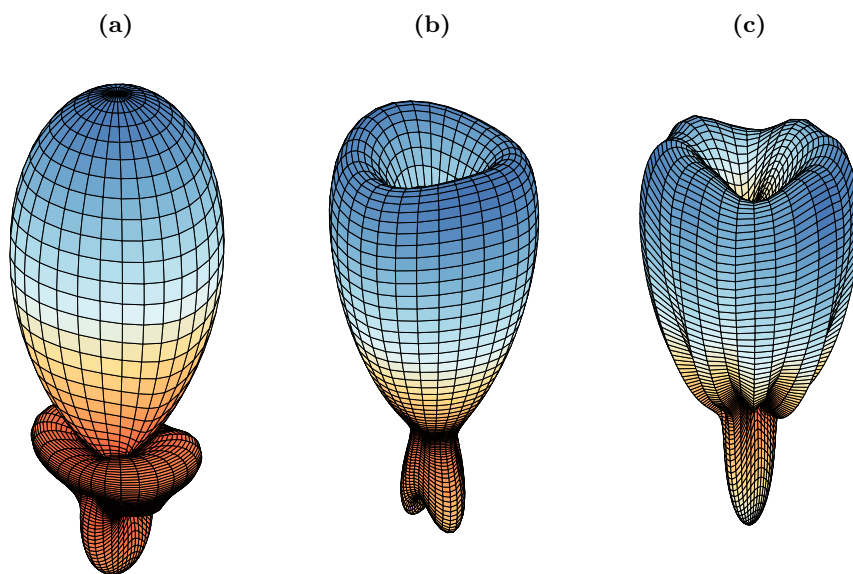


Fig. 8.2. Simulated array patterns for different OAM states

Fig. 8.3 qualitatively shows the azimuthal phase dependence. As expected, the ± 1 states do have exactly one phase dislocation, whereas the ± 2 states have two of them. It can be observed nicely how the phase rotates in opposite directions for the two opposite states. Plot (a) is for the OAM state 0, whereas plots (b) and (d) are for OAM state $+1$ and -1 , respectively, and plots (c) and (e) are for OAM state $+2$ and -2 .

In Fig. 8.2, a ripple can be observed for the OAM state ± 2 . This is even better visible in Fig. 8.3. The ripple causes the figure to be distorted. The ripple is predicted in [25]. In that paper, it is mentioned that the ripple is caused due to a low number of elements.

Instead of increasing the number of elements, the dependence of the array pattern on the diameter is investigated. Thus, additional simulations have been done when the array radius was increased to 55 mm. The results are shown in Fig. 8.4 and Fig. 8.5.

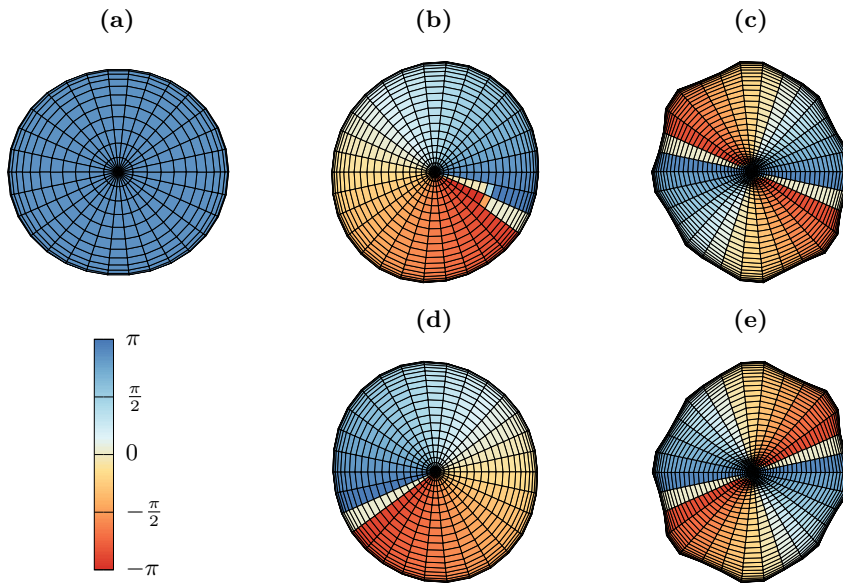


Fig. 8.3. Azimuthal phase dependence of the different OAM states

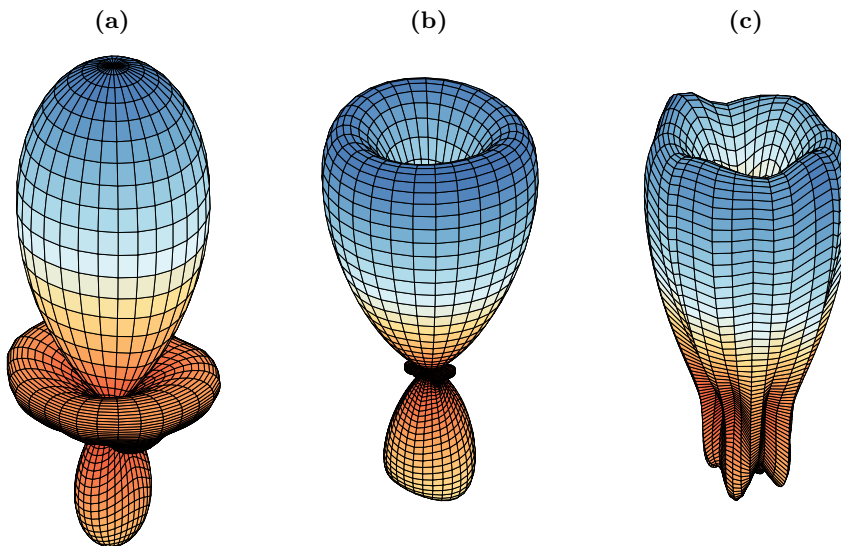


Fig. 8.4. Simulated array patterns for different OAM states, 55 mm array radius

From these plots, it can be observed that the ripple is slightly lower. The OAM state ± 1 is clearly less distorted.

Due to the azimuthal phase distribution of the 3D pattern of the whole array, it can be expected that if an equal array is used at the receiver side, the received signals should have the exact same phase shift between the individual elements. This will be verified by experiment.

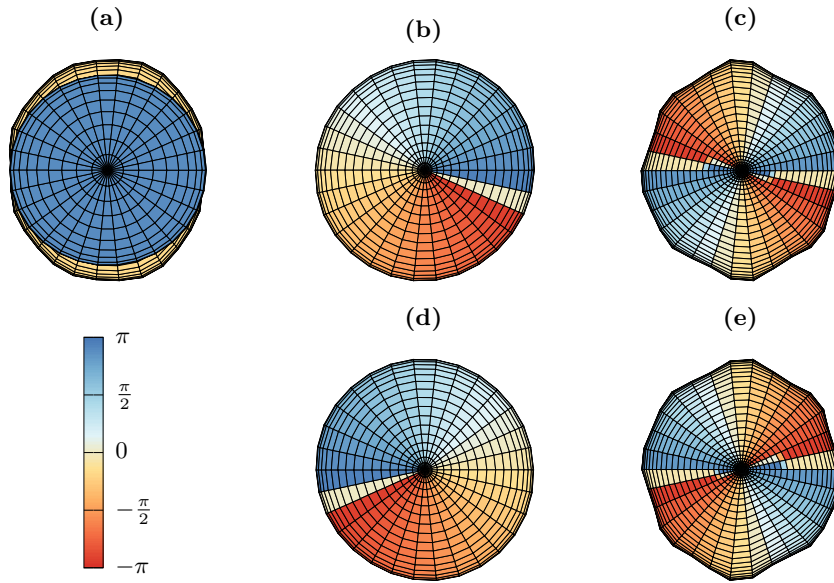


Fig. 8.5. Azimuthal phase dependence of the different OAM states, 55 mm array radius

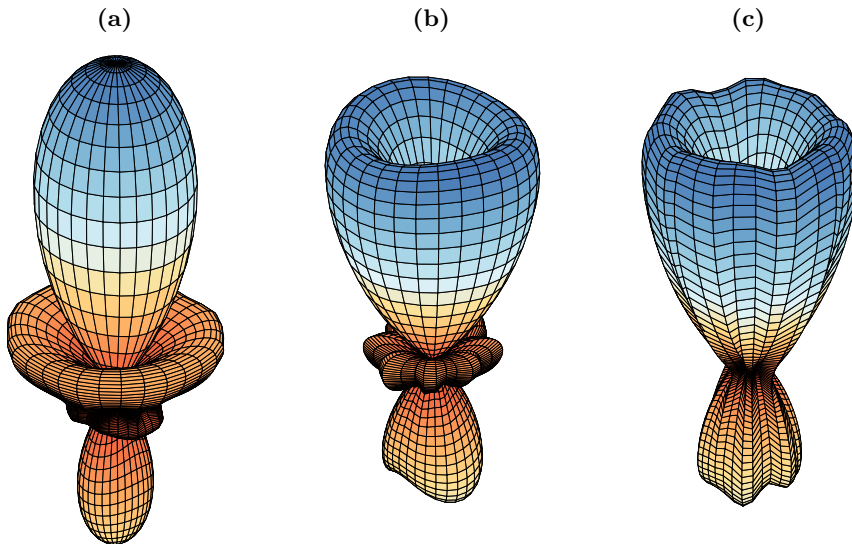


Fig. 8.6. Simulated array patterns for different OAM states, 65 mm array radius

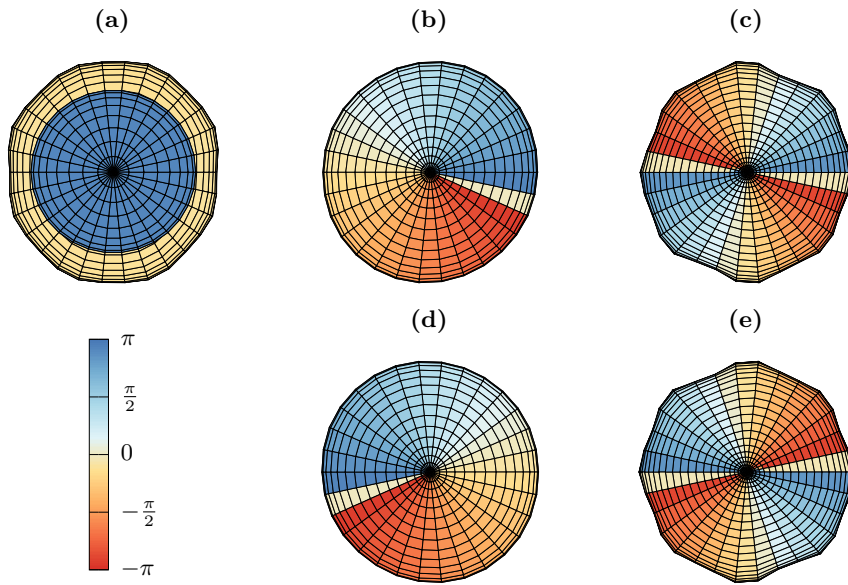


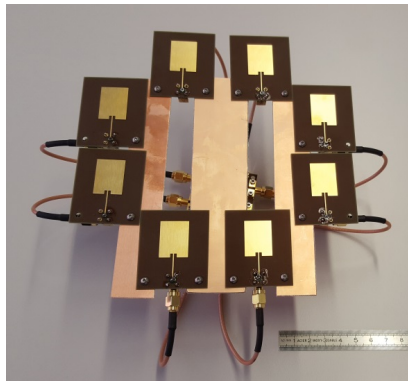
Fig. 8.7. Azimuthal phase dependence of the different OAM states, 65 mm array radius

Experiment setup and measurements

9.1 Construction of the array

Two arrays are constructed. They consist of eight patch antennas each, manufactured on FR4 PC boards as described on page 36. The patch antennas are mounted using strips of PCB raw material. Fig. 9.1 shows how one of the arrays is constructed. The splitter and phase shift network is directly behind the array and is held in place by the eight RG316 coaxial cables.

(a) front view



(b) rear view

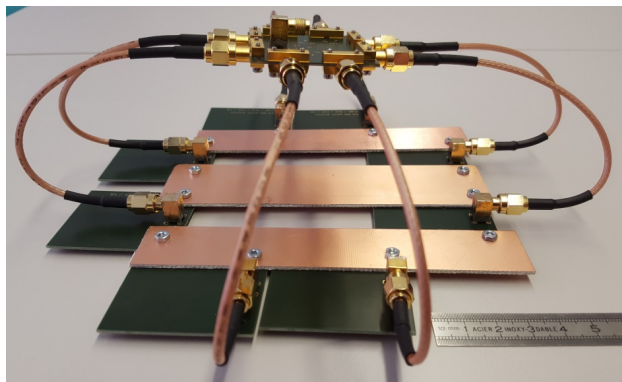


Fig. 9.1. Construction of the 8 element array

9.2 Measurement of the 3D patterns

The antenna array is equipped with the different splitters for the various OAM states and then the 3D pattern is measured using STARLAB. The resulting patterns for the 0° , 45° and 90° splitter are shown in (a), (b) and (c) respectively of Fig. 9.2. As one can see, the patterns are in good accordance with the simulated results.

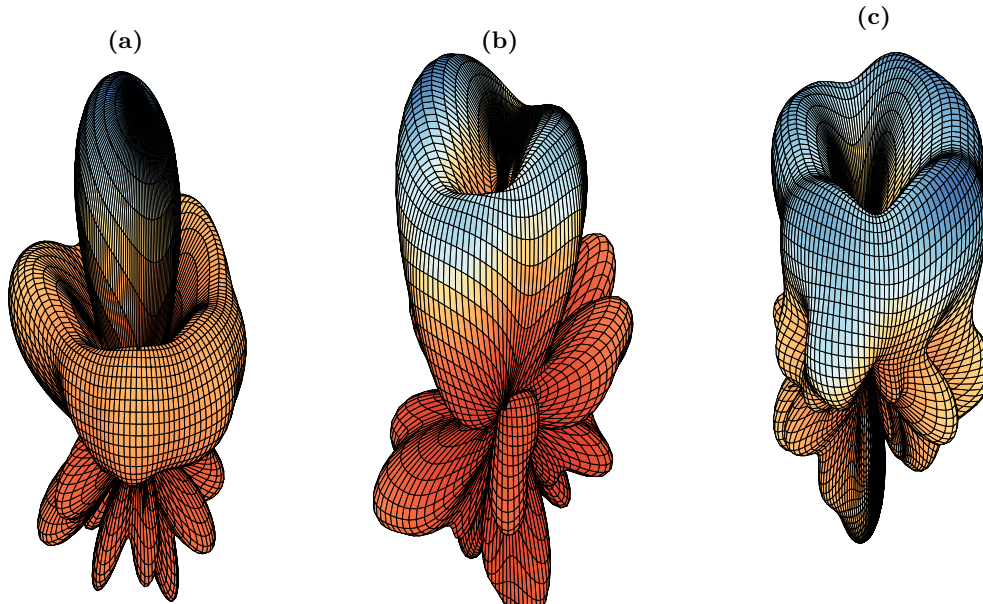


Fig. 9.2. Measured 3D patterns for different OAM states

However, the 135° pattern is in a very bad shape compared to the others, refer to Fig. 9.3.

This could be explained by different reasons:

1. this effect could also be observed in the FEM simulation when the maximal possible OAM state was selected (± 3 in this case).
2. the array is very sensitive to small construction errors (refer also to Sec. 9.4). Thus, the smallest deviation from the ideal circular shape will severely deform the 3D pattern, even though the phase shift between the antenna signals is very accurate, as the measurement of the splitter showed.

Since the 135° pattern is so bad, it was not considered in the following measurements.

9.3 Measurement setup

Fig. 9.4(a) shows a schematic overview of the measurement setup. A Rohde & Schwarz ZVB network analyser is used to measure the magnitude and phase transfer functions. The VNA output power is set to $+30$ dBm and an amplifier is employed in the receive

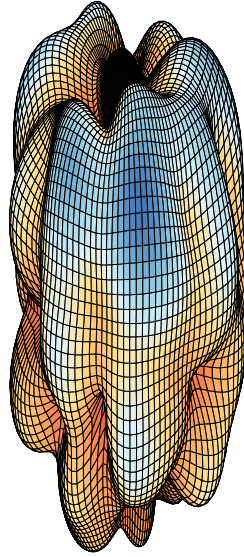


Fig. 9.3. Measured 3D patterns for different OAM states

signal path to add some gain to the wireless link which enhances the measurements. It has been found that especially the phase measurement is extremely difficult if the measurement traces on the VNA are noisy, which can easily happen if the received signal power is very low. The amplifier used is a MINICIRCUITS ZX60-V63+ which works up to 4 GHz, see Fig. 9.4(b).

The antenna arrays are mounted on fibreglass beams with a distance of 1.5 m to the floor. Behind the receiving antenna, an U-shaped absorber wall is installed to prevent the reception of reflections from walls and other equipment behind the receiving antenna. This is shown in Fig. 9.4(c).

The transmitting antenna array sends out an OAM wave with OAM state 0, 1, 2 or 3. The polarisation is vertical since the x -axis of the individual patches (compare with Fig. 7.2) are aligned vertically.

The arrangement of the antennas is done according to IEEE STD-149 “standard test procedures for antennas” because no anechoic chamber is available. See [1] for details. In short, the distance from the antennas to the ground should be

$$h > 4D \quad (9.1)$$

where D is the antenna diameter. In this case, the maximal dimension of the array is 200 mm which gives a height h above ground of at least 800 mm. The antennas are actually mounted 1.5 m above ground.

The distance between the two arrays should be calculated as follows

$$R \geq \max \left\{ \frac{2D^2}{\lambda}, 10\lambda \right\} \quad (9.2)$$

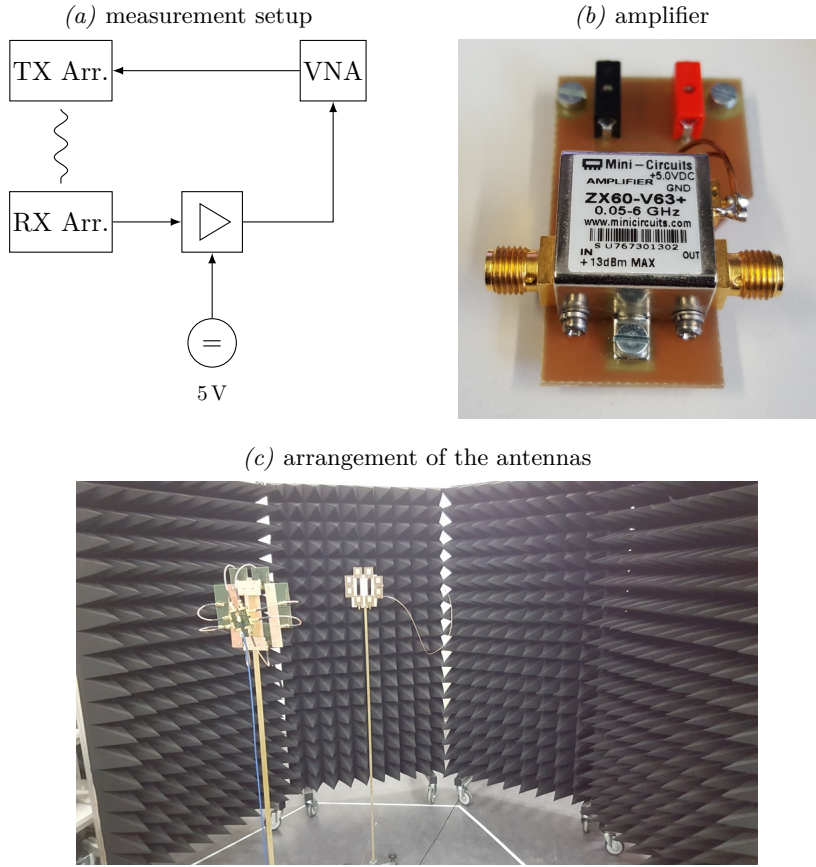


Fig. 9.4. Measurement setup

which gives 933 mm. The effective distance was chosen 1 m. Behind the receiving antenna, there must be free space of at least

$$M_a = \frac{R}{2} \quad (9.3)$$

which was chosen 1 m as well. The lateral free space should be at least

$$M_b = \frac{\sqrt{3}}{2} R \quad (9.4)$$

on both sides; in this case, the lateral distance is much more than 1 m which is more than sufficient for this application. Fig. 9.5 shows the arrangement of the RX and the TX antenna and the distances required.

Not only the phase of the received signal was measured, but also the amplitude when the receiving antenna is moved laterally to different positions. The aim of this measurement is to show the side lobes of the different OAM states. Fig. 9.6 shows the original RX antenna array position (black), whereas the lateral measurements were done on the positions marked in gray.

9.4 Measurement error considerations

At 3.5 GHz, the free-space wave length λ is

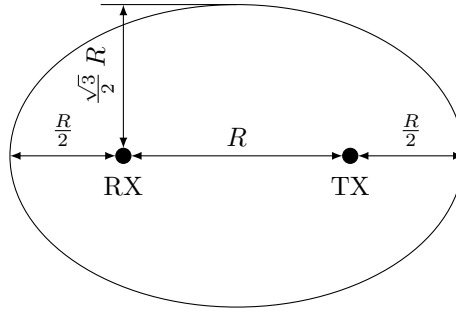


Fig. 9.5. IEEE STD-149 antenna test setup

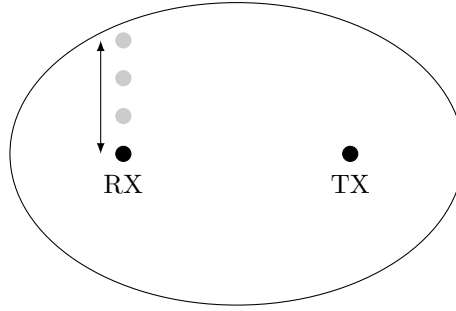


Fig. 9.6. IEEE STD-149 antenna test setup, positions for the lateral power measurement

$$\lambda = \frac{c}{f} \approx 85.7 \text{ mm} \quad (9.5)$$

which equals 360° . A phase shift of 1° thus equals a free-space distance of approx. $238 \mu\text{m}$. On the other hand, if one of the antennas is misplaced by only 4.2 mm , this would already give a 10° phase error.

9.5 Measurement data

Tab. 9.1 shows the values which were measured. The distance between the antennas was varied between 700 mm , which is in the near field according to Eqn. 9.2. Then, the distance was increased to 1 m and 1.5 m , both of which meet the requirement in Eqn. 9.2.

Since the whole system is very prone to phase errors caused by slight misalignment of the antenna arrays, the measurement data from the 0° splitter is used for calibration. Assume the 0° splitter is used at the TX antenna array. If the RX antenna array would be aligned perfectly and the transmitting array as well as the splitter had perfect symmetry, on the receiving side each receiving antenna should have the same phase shift. However, this is not the case due to imperfections of alignment of the two arrays and asymmetry in the arrays themselves. To compensate for this error, the 0° measurement was used as reference measurement. If $\varphi_{n,m}$ is the phase measured at the n -th antenna if splitter m is used at the TX side, the measurements are corrected as follows:

$$\hat{\varphi}_{n,m} = \varphi_{n,m} - \varphi_{n,0} \quad (9.6)$$

distance	ant. #	TX splitter used		
		0°	45°	90°
700 mm	1	-37 dB \angle - 72°	-48 dB \angle 144°	-61 dB \angle - 132°
	2	-39 dB \angle - 77°	-48 dB \angle 112°	-57 dB \angle - 122°
	3	-38 dB \angle - 78°	-49 dB \angle 72°	-56 dB \angle - 149°
	4	-37 dB \angle - 74°	-50 dB \angle 27°	-59 dB \angle - 165°
	5	-38 dB \angle - 88°	-49 dB \angle - 23°	-67 dB \angle - 170°
	6	-37 dB \angle - 72°	-49 dB \angle - 54°	-62 dB \angle - 160°
	7	-38 dB \angle - 86°	-54 dB \angle - 103°	-59 dB \angle - 150°
	8	-38 dB \angle - 77°	-54 dB \angle - 155°	-59 dB \angle - 165°
1 m	1	-41 dB \angle 34°	-57 dB \angle - 103°	-61 dB \angle - 54°
	2	-42 dB \angle 30°	-57 dB \angle - 141°	-62 dB \angle - 36°
	3	-42 dB \angle 31°	-57 dB \angle 179°	-60 dB \angle - 42°
	4	-41 dB \angle 39°	-57 dB \angle 123°	-62 dB \angle - 60°
	5	-42 dB \angle 44°	-56 dB \angle 84°	-71 dB \angle - 44°
	6	-41 dB \angle 39°	-54 dB \angle 44°	-62 dB \angle - 51°
	7	-43 dB \angle 27°	-60 dB \angle 8°	-66 dB \angle - 96°
	8	-42 dB \angle 35°	-62 dB \angle - 35°	-65 dB \angle - 84°
1.5 m	1	-45 dB \angle 35°	-65 dB \angle - 110°	-66 dB \angle - 69°
	2	-45 dB \angle 26°	-64 dB \angle - 155°	-66 dB \angle - 45°
	3	-45 dB \angle 33°	-63 dB \angle 171°	-64 dB \angle - 39°
	4	-45 dB \angle 39°	-66 dB \angle 133°	-65 dB \angle - 59°
	5	-45 dB \angle 33°	-61 dB \angle 88°	-68 dB \angle - 60°
	6	-45 dB \angle 36°	-62 dB \angle 43°	-67 dB \angle - 63°
	7	-46 dB \angle 32°	-67 dB \angle 2°	-68 dB \angle - 85°
	8	-45 dB \angle 35°	-67 dB \angle - 40°	-64 dB \angle - 59°

Table 9.1. Measurement data

This yields the measurement data shown in Tab. 9.2.

For the lateral displacement of the RX antenna, the measurement data is shown in Tab. 9.3.

9.6 Interpretation of the measurement results

Following observations can be made from the measurements shown in Tab. 9.1 and Tab. 9.2:

- the received power decreases as the distance is increased. Looking at the OAM state 0, the $\frac{1}{r^2}$ rule can easily be seen, which states that

$$\frac{P_2}{P_1} = \left(\frac{R_1}{R_2}\right)^2 \quad (9.7)$$

dist.	ant. #	TX splitter used		
		0°	45°	90°
700 mm	1	-37 dB \angle 0°	-48 dB \angle - 144°	-61 dB \angle - 132°
	2	-39 dB \angle 0°	-48 dB \angle - 171°	-57 dB \angle - 122°
	3	-38 dB \angle 0°	-49 dB \angle 150°	-56 dB \angle - 149°
	4	-37 dB \angle 0°	-50 dB \angle 101°	-59 dB \angle - 165°
	5	-38 dB \angle 0°	-49 dB \angle 65°	-67 dB \angle - 170°
	6	-37 dB \angle 0°	-49 dB \angle 18°	-62 dB \angle - 160°
	7	-38 dB \angle 0°	-54 dB \angle - 17°	-59 dB \angle - 150°
	8	-38 dB \angle 0°	-54 dB \angle - 78°	-59 dB \angle - 165°
1 m	1	-41 dB \angle 0°	-57 dB \angle - 137°	-61 dB \angle - 54°
	2	-42 dB \angle 0°	-57 dB \angle - 171°	-62 dB \angle - 36°
	3	-42 dB \angle 0°	-57 dB \angle 148°	-60 dB \angle - 42°
	4	-41 dB \angle 0°	-57 dB \angle 84°	-62 dB \angle - 60°
	5	-42 dB \angle 0°	-56 dB \angle 40°	-71 dB \angle - 44°
	6	-41 dB \angle 0°	-54 dB \angle 5°	-62 dB \angle - 51°
	7	-43 dB \angle 0°	-60 dB \angle - 19°	-66 dB \angle - 96°
	8	-42 dB \angle 0°	-62 dB \angle - 70°	-65 dB \angle - 84°
1.5 m	1	-45 dB \angle 0°	-65 dB \angle - 145°	-66 dB \angle - 69°
	2	-45 dB \angle 0°	-64 dB \angle 179°	-66 dB \angle - 45°
	3	-45 dB \angle 0°	-63 dB \angle 138°	-64 dB \angle - 39°
	4	-45 dB \angle 0°	-66 dB \angle 94°	-65 dB \angle - 59°
	5	-45 dB \angle 0°	-61 dB \angle 55°	-68 dB \angle - 60°
	6	-45 dB \angle 0°	-62 dB \angle 7°	-67 dB \angle - 63°
	7	-46 dB \angle 0°	-67 dB \angle - 30°	-68 dB \angle - 85°
	8	-45 dB \angle 0°	-67 dB \angle - 75°	-64 dB \angle - 59°

Table 9.2. Measurement data, calibrated

which would result in a power drop of 6.6 dB if the distance is increased from 700 mm to 1.5 m. From 700 mm to 1 m the drop should be approx. 3.1 dB, this value is also verified from the tables with ease.

- the mean absolute phase difference between the individual array elements is 8.5°. This is a good value and comes close to the ideal value of 0° if the ruggedness of the experiment setup is considered.
- For the 0° and the 45° TX splitters, the phase behaves exactly as expected. However, the 90° OAM state could not be measured directly. A possible reason for this is that the RX antenna array is too small due to the beam divergence. To verify this, the lateral measurement was done.
- For the lateral RX power measurement, the results are exactly as expected. The 0° OAM state has its maximum power in the centre (0 cm displacement) and the

dist.	lateral dist.	TX splitter used		
		0°	45°	90°
700 mm	0 cm	-37 dB	-49 dB	-61 dB
	10 cm	-43 dB	-43 dB	-57 dB
	20 cm	-53 dB	-43 dB	-50 dB
	30 cm	-57 dB	-48 dB	-48 dB
	40 cm	-53 dB	-53 dB	-47 dB
	50 cm	-53 dB	-60 dB	-51 dB
	60 cm	-54 dB	-70 dB	-55 dB
	70 cm	-58 dB	-71 dB	-56 dB
1 m	0 cm	-41 dB	-63 dB	-62 dB
	10 cm	-43 dB	-50 dB	-61 dB
	20 cm	-47 dB	-47 dB	-56 dB
	30 cm	-55 dB	-47 dB	-53 dB
	40 cm	-64 dB	-48 dB	-52 dB
	50 cm	-61 dB	-50 dB	-52 dB
	60 cm	-58 dB	-53 dB	-53 dB
	70 cm	-55 dB	-58 dB	-54 dB
1.5 m	0 cm	-45 dB	-55 dB	-67 dB
	10 cm	-46 dB	-44 dB	-69 dB
	20 cm	-48 dB	-43 dB	-63 dB
	30 cm	-50 dB	-45 dB	-58 dB
	40 cm	-52 dB	-50 dB	-55 dB
	50 cm	-57 dB	-56 dB	-55 dB
	60 cm	-66 dB	-64 dB	-56 dB
	70 cm	-67 dB	-69 dB	-56 dB

Table 9.3. Measurement data, lateral displacement

received signal power decreases with increasing lateral displacement. This is in good accordance with the expectation, if it is compared with the 3D pattern of the 0° array (Fig. 9.2). One can also see that the power slightly increases again with increasing lateral displacement. This is due to the small side lobe of the 0° array.

- The 45° and 90° arrays behave in the lateral power measurement also as expected. In the centre (0 cm displacement), the received signal power is at its minimum and increases with increasing lateral displacement to decrease then after a certain limit. This is due to the deep null in the centre of the OAM states 1 and 2 and the increasing power is due to the shape of the 3D pattern which looks like a sort of cup. The increasing power is due to the walls of the “cup” and the minimum power in the centre is the hole in the middle of the “cup”. Compare again with the patterns shown in Fig. 9.2.

Lessons learned and outlook

A lot of time was used for the design of the patch antennas. It has been found to be very difficult to obtain a good match between the simulation and the real measurements. The same applied to the phase shifting network. Since it has been found that the Laser manufacturing tool available at the HSLU is not precise enough, the PCBs were manufactured by PCB pool, which only has FR4 material available. Thus, a redesign had to be done for these networks, which also cost a lot of time.

Due to these reasons, it was later not possible to do as much measurements as was desired. Furthermore, the mounting of the antennas turned out to be much more complicated as it was planned.

A third problem resulted from the measurement of the transfer function: for each measurement, it was necessary to disconnect the SMA connector and re-connect it on the next array element. Due to this, the array had to be touched before each measurement, which gives rise to small positional disturbances and thus introduces additional phase errors.

For a further project, following suggestions result from the above mentioned drawbacks:

- A very stiff frame should be constructed of dielectric material, e.g. fibreglass, to allow a precise mounting of the antennas. It should allow to measure the distance between the two arrays and it should ensure that both arrays are parallel to each other.
- A electronic switching device should be considered which allows to connect each array element with the network analyser without touching the arrays. Only with such a device it is possible to ensure that the positions of the arrays are precise enough. As was shown in Sec. 9.4, a slight offset of only 4 mm in one direction already gives rise to 10° of phase error.
- It would be nice to have an anechoic chamber available for the measurements.

10.1 Conclusion

The design of inset fed microstrip patch antennas was investigated and FEM simulations were done to verify the return loss and the pattern of the patches. The construction of a phase shifting power splitter was also investigated; several prototypes were fabricated. A phased array of 8 elements has been built, its 3D pattern was measured and simulated. The qualitative accordance of the measured and simulated 3D patterns was shown. Two of these arrays, one of these equipped with a phase shifting and power splitter network, were installed and a near-field (700 mm distance) and far-field (≥ 1 m) measurement of the transfer coefficient between the two arrays was done. The measurements for the OAM states 0 and 1 were in good accordance with the expectations; the OAM states 2 and 3 could not be measured accurately. The orthogonality of two different OAM states was shown using a numerical example.

Due to the above points, the project can be considered as a partial success. Unfortunately, the project was in the author's point of view not as successful as it should have been. Manufacturing of the components, the measurement setup and the measurements itself is much more difficult than first thought of.

10.2 Outlook

Since two different OAM states – e.g. state 0 and state 1 – are orthogonal to each other, as the numerical example showed, they could be used for a sort of diversity which should be called *Orbital Angular Momentum Diversity*. It could be used similar to the polarisation diversity. This means, a transmitter is capable of transmitting both OAM states -1 and $+1$ at the same time. The receiver could then receive that state which has a better SNR, exactly like it is done for the polarisation diversity.

In this section, a short proposal for such an OAM transmitter is made. For the sake of simplicity, arrays with only 4 elements are used, giving the possibility to use OAM states 0 and ± 1 . Fig. 10.1 shows a block diagram of the proposed transmitter.

The transmitter has four outputs, one for each array element. The outputs are fed by the combiners. Each combiner has two inputs, one of which is connected to a $+90^\circ$ phase shifter, whereas the other input is connected to a -90° phase shifter. The positive phase shift lets the array emit the OAM state $+1$, whereas the negative phase shift will produce OAM state -1 .

The phase shifters are fed by the boxes labeled “S”. This is, in this case, a simple 0° 4-way power splitter. The power splitters each have one input, in this case these are called inputs A and B. A signal fed to input A will be transmitted using OAM state 1 and the signal fed into input B will be transmitted using OAM state -1 .

The transmitter can select on which input the data is to be transmitted. In this special case, the phase shifts are exactly 180° out of phase, which means that it

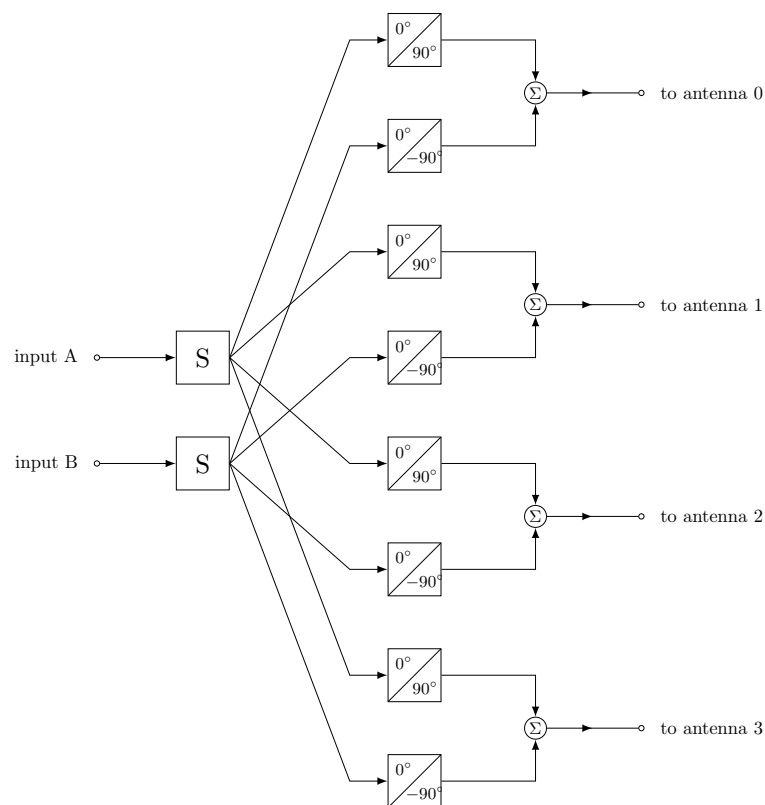


Fig. 10.1. Proposal for an OAM diversity transmitter

will not be possible to transmit two OAM states at the same time. However, if, for instance, the $+90^\circ$ phase shifter is replaced with a 0° shifter, then it should be possible to transmit both OAM states at the same time.

The 90° phase shift has the advantage that it can easily be implemented with a digital filter with aid of the Hilbert transform. Thus, it could be possible to implement the whole transmitter using DSP techniques and use mixers for the RF fronted only.

Appendix

List of Tables

3.1 Overview of splitter topologies and their properties	13
3.2 Comparison between several commercially available splitters	16
4.1 Numerical results	19
5.1 Specification of the available base materials for PCBs.....	24
6.1 Magnitude and phase of the manufactured splitters	26
6.2 calculated phase difference between the output ports of the splitters	27
7.1 Polynomial coefficients for the inset feed calculation	31
7.2 Calculated dimensions for the patch antenna variants.....	33
7.3 Optimised dimensions	33
7.4 Dimensions of the redesigned patch antenna	35
9.1 Measurement data	48
9.2 Measurement data, calibrated	49
9.3 Measurement data, lateral displacement	50

List of Figures

2.1	Types of phased arrays	5
2.2	Schematic overview of a linear antenna array	6
2.3	Refraction of a wave at an air-water interface	7
2.4	Converting a linear to a circular array	8
2.5	Comparison of different OAM states of a four element array	10
2.6	Comparison of different OAM states of a eight element array	11
2.7	Vector field plots for different OAM states, linear and circular polarisation	12
3.1	Some topologies of power splitters.....	14
3.2	An 8-way splitter for the feed network	15
3.3	Numbering scheme	15
3.4	Transmission and reflection characteristics of the MINICIRCUITS device.....	17
3.5	Output balance of the MINICIRCUITS device	17
6.1	CAD drawing of the 0° splitter	25
6.2	CAD drawings of the different PCB variants, to scale	27
6.3	Photographs of the manufactured splitters	28
7.1	Geometry of the patch antenna with inset microstrip feed	29
7.2	Analysis of the polarisation of a patch antenna	30
7.3	Polarisation of the patch antenna	30
7.4	Simulated return loss of the patch antenna variants	33
7.5	Comparison of the return loss of the original (dashed lines) and the optimised patch antenna geometries (straight lines)	34
7.6	Photograph of the manufactured patch antenna	34
7.7	Measured scattering parameter of the manufactured antenna.....	35
7.8	Photograph of the redesigned patch antenna	35
7.9	Measured scattering parameter of the manufactured antenna.....	36
7.10	How the antenna radiation pattern is measured.....	36
7.11	Measured radiation pattern of the patch antenna.....	37
8.1	Orientation of the array for the simulation	39
8.2	Simulated array patterns for different OAM states	39
8.3	Azimuthal phase dependence of the different OAM states	40
8.4	Simulated array patterns for different OAM states, 55 mm array radius	40
8.5	Azimuthal phase dependence of the different OAM states, 55 mm array radius	41
8.6	Simulated array patterns for different OAM states, 65 mm array radius	41
8.7	Azimuthal phase dependence of the different OAM states, 65 mm array radius	42
9.1	Construction of the 8 element array.....	43

9.2 Measured 3D patterns for different OAM states	44
9.3 Measured 3D patterns for different OAM states	45
9.4 Measurement setup	46
9.5 IEEE STD-149 antenna test setup	47
9.6 IEEE STD-149 antenna test setup, positions for the lateral power measurement	47
10.1 Proposal for an OAM diversity transmitter	53

A

Datasheets

Surface Mount

Power Splitter/Combiner

SP-2L+

2 Way-0° 50Ω

2700 to 4000 MHz



CASE STYLE: CA531
PRICE: \$ 0.96 ea. QTY (20)

+RoHS Compliant

The +Suffix identifies RoHS Compliance. See our web site for RoHS Compliance methodologies and qualifications



Available Tape and Reel at no extra cost

Reel Size	Devices/Reel
7"	20, 50, 100, 200, 500, 1000

Maximum Ratings

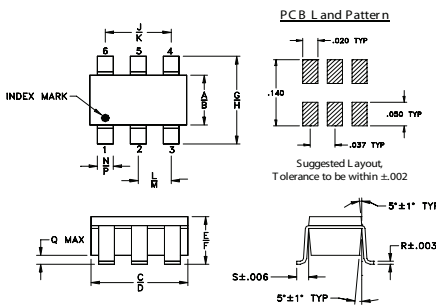
Operating Temperature	-40°C to 85°C
Storage Temperature	-65°C to 150°C
Power Input (as a splitter)	0.75W max.
Internal Dissipation	0.375W max.

Permanent damage may occur if any of these limits are exceeded.

Pin Connections

SUM PORT	5
PORT 1	1
PORT 2	3
GROUND	2,4,6

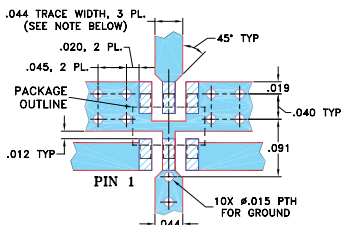
Outline Drawing



Outline Dimensions (inch)

A	B	C	D	E	F	G	H	J	K	L	M	N	P	Q	R	S	wt
.052	.067	.106	.122	.035	.064	.087	.118	.067	2.11	0.84	1.07	0.30	0.51	0.30	0.15	0.46	0.020
1.32	1.70	2.69	3.10	0.89	1.63	2.21	3.00	1.70									grams

Demo Board MCL P/N: TB-374 Suggested PCB Layout (PL-232)



- NOTES: 1. TRACE WIDTH IS SHOWN FOR ROGERS RO4350B WITH DIELECTRIC THICKNESS .020" ± .0015"; COPPER: 1/2 OZ. EACH SIDE. FOR OTHER MATERIALS TRACE WIDTH MAY NEED TO BE MODIFIED.
2. BOTTOM SIDE OF THE PCB IS CONTINUOUS GROUND PLANE.
- DENOTES PCB COPPER LAYOUT WITH SMOBC (SOLDER MASK OVER BARE COPPER)
 - DENOTES COPPER LAND PATTERN FREE OF SOLDER MASK

Features

- low insertion loss, 0.75 dB typ.
- good isolation, 18 dB typ.
- good output VSWR, 1.3:1 typ.
- excellent power handling, 1.5W
- small size
- aqueous washable

Applications

- WIMAX
- WIMAX local oscillator

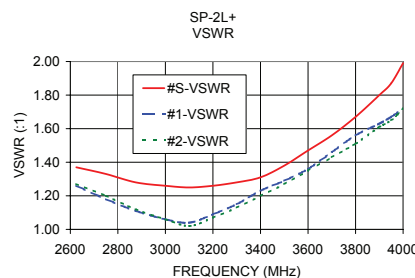
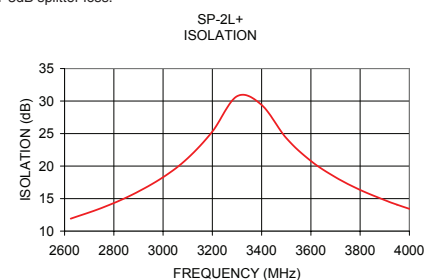
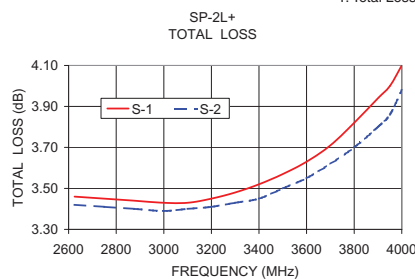
Electrical Specifications

FREQ. RANGE (MHz)	ISOLATION (dB)		INSERTION LOSS (dB) ABOVE 3.0 dB		PHASE UNBALANCE (Degrees)	AMPLITUDE UNBALANCE (dB)	VSWR (:1)	
	Typ.	Min.	Typ.	Max.			S-Port Typ.	Output Ports Typ.
2700-4000	18	10	0.75	1.4	8	0.3	1.5	1.3

Typical Performance Data

Frequency (MHz)	Total Loss ¹ (dB)		Amplitude Unbalance (dB)	Isolation (dB)	Phase Unbalance (deg.)	VSWR S	VSWR 1	VSWR 2
	S-1	S-2						
2625.00	3.46	3.42	0.03	11.91	0.85	1.37	1.26	1.27
2750.00	3.45	3.41	0.04	13.55	0.95	1.33	1.18	1.20
2875.00	3.44	3.40	0.04	15.61	0.96	1.28	1.11	1.12
3000.00	3.43	3.39	0.03	18.28	0.93	1.26	1.06	1.06
3100.00	3.43	3.40	0.02	21.21	1.01	1.25	1.04	1.02
3200.00	3.45	3.41	0.04	25.31	1.07	1.26	1.09	1.07
3300.00	3.48	3.43	0.05	30.74	1.11	1.28	1.15	1.13
3400.00	3.52	3.45	0.06	29.40	1.11	1.31	1.23	1.20
3500.00	3.57	3.50	0.07	24.32	1.15	1.38	1.29	1.27
3600.00	3.63	3.55	0.08	20.79	1.26	1.47	1.36	1.35
3700.00	3.71	3.62	0.10	18.28	1.33	1.56	1.46	1.43
3800.00	3.82	3.70	0.12	16.33	1.25	1.67	1.56	1.51
3900.00	3.94	3.80	0.14	14.76	1.12	1.80	1.63	1.61
3950.00	4.00	3.86	0.13	14.06	0.97	1.87	1.67	1.65
4000.00	4.10	3.98	0.13	13.43	0.99	1.99	1.72	1.72

1. Total Loss = Insertion Loss + 3dB splitter loss.



electrical schematic



Mini-Circuits
ISO 9001 ISO 14001 AS 9100 CERTIFIED

P.O. Box 350166, Brooklyn, New York 11235-0003 (718) 934-4500 Fax (718) 332-4661 The Design Engineers Search Engine Provides ACTUAL Data Instantly at minicircuits.com

IF/RF MICROWAVE COMPONENTS

Notes: 1. Performance and quality attributes and conditions not expressly stated in this specification sheet are intended to be excluded and do not form a part of this specification sheet. 2. Electrical specifications and performance data contained herein are based on Mini-Circuit's applicable established test performance criteria and measurement instructions. 3. The parts covered by this specification sheet are subject to Mini-Circuits standard limited warranty and terms and conditions (collectively, "Standard Terms"); Purchasers of this part are entitled to the rights and benefits contained therein. For a full statement of the Standard Terms and the exclusive rights and remedies thereunder, please visit Mini-Circuits' website at www.minicircuits.com/MCLStore/terms.jsp.

For detailed performance specs & shipping online see web site

REV. A
M127604
ED-12593/3/4
SP-2L+
RS/LC/CP/AM
120509

References

- [1] “IEEE standard test procedures for antennas.”
- [2] A. M. Abbosh, “Compact Tunable Reflection Phase Shifters Using Short Section of Coupled Lines,” *IEEE Trans. Microw. Theory Tech.*, vol. 60, no. 8, pp. 2465–2472, aug 2012.
- [3] B. A. Arand and M. Amrollahzadeh, “An S band low cost 6-bit PIN diode phase shifter,” in *7th International Symposium on Telecommunications (IST'2014)*. Institute of Electrical & Electronics Engineers (IEEE), sep 2014.
- [4] Q. Bai, A. Tennant, and B. Allen, “Experimental circular phased array for generating OAM radio beams,” *Electronics Letters*, vol. 50, no. 20, pp. 1414–1415, sep 2014.
- [5] R. N. Damman, J. T. Rayno, and S. K. Sharma, “Beam steering performance of a wideband modified e-shape microstrip patch antenna array,” in *Proceedings of the 2012 IEEE International Symposium on Antennas and Propagation*. Institute of Electrical & Electronics Engineers (IEEE), jul 2012.
- [6] R. Douville and D. James, “Experimental study of symmetric microstrip bends and their compensation,” *IEEE Transactions on Microwave Theory and Techniques*, vol. 26, no. 3, pp. 175–182, mar 1978.
- [7] R. S. Elliott, *Antenna Theory & Design*. Wiley-IEEE Press, 2003.
- [8] R. Garver, “Broad-band diode phase shifters,” *IEEE Trans. Microw. Theory Tech.*, vol. 20, no. 5, pp. 314–323, may 1972.
- [9] T. Gockel, *Form der wissenschaftlichen Ausarbeitung*. Heidelberg: Springer-Verlag, 2008, additional material available at <http://www.formbuch.de>.
- [10] F. Gustrau, *Hochfrequenztechnik – Grundlagen der mobilen Kommunikationstechnik*. Hanser-Verlag, 2013.

- [11] R. F. Harrington, *Time-Harmonic Electromagnetic Fields*, D. G. Dudley, Ed. Wiley, 2001.
- [12] A. Helaly, A. Sebak, and L. Shafai, "Phase centre movement in linear phased array antennas," in *International Symposium on Antennas and Propagation Society, Merging Technologies for the 90's*. Institute of Electrical & Electronics Engineers (IEEE), 1990.
- [13] N. Irfan, "Design of a microstrip-line-fed inset patch antenna for RFID applications," *IJET*, vol. 4, no. 5, pp. 558–561, 2012.
- [14] S. O. Kasap, *Principles of Electronic Materials and Devices*. McGraw Hill, 2006.
- [15] H. R. Kaupp, "Characteristics of microstrip transmission lines," *IEEE Transactions on Electronic Computers*, vol. EC-16, no. 2, pp. 185–193, apr 1967.
- [16] D. Klymyshyn, S. Kumar, and A. Mohammadi, "Linear reflection phase shifter with optimised varactor gamma," *Electron. Lett.*, vol. 33, no. 12, p. 1054, 1997.
- [17] M. Kori and S. Mahapatra, "Switched reflection phase shifter," *Electron. Lett.*, vol. 22, no. 10, pp. 550–551, may 1986.
- [18] J. D. Kraus, *Antennas*. McGraw-Hill, 1988.
- [19] J.-S. Lee, T.-L. Song, J.-K. Du, and J.-G. Yook, "Near-field to far-field transformation based on stratton-chu fomula for EMC measurements," in *2013 IEEE Antennas and Propagation Society International Symposium (APSURSI)*. Institute of Electrical & Electronics Engineers (IEEE), jul 2013.
- [20] L. L. Liou, D. M. Lin, J. T. Tsui, J. Buck, M. Longbrake, J. McCann, P. Buxa, and T. Dalrymple, "Angle of arrival measurement using wideband linear phased array," in *Proceedings of the IEEE 2009 National Aerospace & Electronics Conference (NAECON)*. Institute of Electrical & Electronics Engineers (IEEE), jul 2009.
- [21] G. Lynes, G. Johnson, B. Huckleberry, and N. Forrest, "Design of a broad-band 4-bit loaded switched-line phase shifter," *IEEE Trans. Microw. Theory Tech.*, vol. 22, no. 6, pp. 693–697, jun 1974.
- [22] J. Ma, J. Du, X. Hu, and J. Wang, "Design of integrated circularly polarized orbital angular momentum (OAM) beam emitter using microring with interleaved tailored angular gratings," in *CLEO: 2015*. The Optical Society, 2015.

- [23] L. G. Maloratsky, “Electrically tunable switched-line diode phase shifters,” *High Frequency Electronics*, 2010.
- [24] G. L. Matthaei, L. Young, and E. M. T. Jones, *Microwave filters, impedance-matching networks, and coupling structures*, ser. The Artech House microwave library. Dedham: Artech House books, 1980.
- [25] S. M. Mohammadi, L. K. S. Daldorff, J. E. S. Bergman, R. L. Karlsson, B. Thide, K. Forozesh, T. D. Carozzi, and B. Isham, “Orbital angular momentum in radio – a system study,” *IEEE Trans. Antennas Propag.*, vol. 58, no. 2, pp. 565–572, Dec. 2009.
- [26] K. Nakada, T. Marumoto, and R. Iwata, “Stub switched phase shifter,” in *IEEE Antennas and Propagation Society International Symposium*. Institute of Electrical & Electronics Engineers (IEEE), 2000.
- [27] J. Peatross and M. Ware, *Physics of Light and Optics*. Brigham Young University, 2014.
- [28] D. M. Pozar, *Microwave Engineering*. Wiley, 2011.
- [29] S. N. A. Prince, P. Muthukumaran, and N. Jagatheesh, “Design and implementation of two 1-bit switched line phase shifter,” in *2014 IEEE International Conference on Advanced Communications, Control and Computing Technologies*. Institute of Electrical & Electronics Engineers (IEEE), may 2014.
- [30] B. E. A. Saleh and M. C. Teich, *Fundamentals of Photonics*. Wiley, 2007.
- [31] A. Tennant and B. Allen, “Generation of radio frequency OAM radiation modes using circular time-switched and phased array antennas,” in *2012 Loughborough Antennas & Propagation Conference (LAPC)*. Institute of Electrical & Electronics Engineers (IEEE), nov 2012.
- [32] B. Thidé, H. Then, J. Sjöholm, K. Palmer, J. Bergman, T. D. Carozzi, Y. N. Istomin, N. H. Ibragimov, and R. Khamitova, “Utilization of photon orbital angular momentum in the low-frequency radio domain,” *Phys. Rev. Lett.*, vol. 99, p. 087701, Aug. 2007.
- [33] U. Tietze, C. Schenk, and E. Gamm, *Halbleiter-Schaltungstechnik*. Springer, 2012.
- [34] S. E. Valavan, D. Tran, A. G. Yarovoy, and A. G. Roederer, “Dual-band linear phased array in k-band,” in *2014 44th European Microwave Conference*. Institute of Electrical & Electronics Engineers (IEEE), oct 2014.

- [35] P. Vieira, P. Queluz, and A. Rodrigues, “LTE spectral efficiency using spatial multiplexing MIMO for macro-cells,” in *2008 2nd International Conference on Signal Processing and Communication Systems*. IEEE, dec 2008.
- [36] R. Waterhouse, *Microstrip Patch Antennas: A Designer’s Guide*. Springer, 2010.
- [37] A. Weisshaar and V. Tripathi, “Perturbation analysis and modeling of curved microstrip bends,” *IEEE Transactions on Microwave Theory and Techniques*, vol. 38, no. 10, pp. 1449–1454, 1990.
- [38] Y. Yan, G. Xie, M. P. J. Lavery, H. Huang, N. Ahmed, C. Bao, Y. Ren, Y. Cao, L. Li, Z. Zhao, A. F. Molisch, M. Tur, M. J. Padgett, and A. E. Willner, “High-capacity millimetre-wave communications with orbital angular momentum multiplexing,” *Nat Comms*, vol. 5, p. 4876, sep 2014.

Glossary

Altium Designer	is a CAD software for PCB layout.
CAD	computer aided design.
COMSOL	a software program for finite element physics simulation.
Empire	is a software for simulation of antennas.
HP	Hewlett Packard.
MATLAB	a software program for mathematical calculations.
MEMS	are micro-electromechanical devices.
OAM	orbital angular momentum.
PCB	a <i>printed circuit board</i> .
PIN	a PIN diode is a special type of a diode used for switching of RF signals.
Rogers	is a manufacturer of PC board base material.
SMA	means “sub-miniature A”. It is a form of coaxial connector.
SMT	means “surface mount technology”.
SPDT	is a single-pole double-throw switch.
SPP	is a <i>spiral phase plate</i> .
Starlab	a device for the measurement of antenna patterns.